Aus der Klinik und Poliklinik für Neurologie

der Universitätsmedizin der Johannes Gutenberg-Universität Mainz

Differenzierte Motoneurone als Modell zur Untersuchung von Stoffwechselvorgängen im Zusammenhang mit der Charcot-Marie-Tooth Erkrankung

(Differentiated Motoneurons as a Model to Study Metabolic Function in Charcot-Marie-Tooth Disease)

Inauguraldissertation

zur Erlangung des Doktorgrades der Medizin

der Universitätsmedizin

der Johannes Gutenberg-Universität Mainz

Vorgelegt von

Lisa Pflaum

aus Tübingen

Mainz, 2021

Wissenschaftlicher Vorstand:

1. Gutachter:

2. Gutachter:

Tag der Promotion: 12. Juli 2022

Content

Zusammenfassung

Mitofusin 2 (MFN2) ist ein mitochondriales Protein, dessen Mutation $MFN2^{R94Q}$ die Motoneuronerkrankung Charcot-Marie-Tooth (CMT) 2A verursacht. Das Ziel dieser Arbeit war es, murine embryonale Stammzellen zu Motoneuronen zu differenzieren und in diesen Motoneuronen zu untersuchen, ob die Überexpression der Mutation zu Veränderungen im Stoffwechsel der Zellen führt.

Die verwendeten embryonalen Stammzellen waren mit einem Differenzierungsmodul unter der Kontrolle eines "Tet-on"-Systems ausgestattet. Ich konnte bestätigen, dass die Zugabe von Doxycyclin und den entsprechenden strukturbildenden Faktoren zu diesen Zellen zur Ausbildung von postmitotischen Motoneuronen führt. Die selektive Überexpression von MFN2 und seiner mutierten Version in den erwähnten neuronalen Zellen konnte ich daraufhin mit Hilfe eines "DIO"-Expressionssystems, das durch einen neuronenspezifischen Hb9-Promoter reguliert wurde, durchführen. Von den in dieser Arbeit verglichenen Substanzen zur Transfektion war "Lipofectamine 2000" am besten geeignet.

Die Auswirkung der oben genannten Mutation auf den Stoffwechsel der Neurone, insbesondere auf die ATP- und Laktatkonzentration, habe ich mit genetisch kodierten FRET-Sensoren untersucht. Durch Analyse der transfizierten Zellen unter dem Konfokalmikroskop konnte ich die erfolgreiche Expression der genetischen Indikatoren in den differenzierten Motoneuronen belegen. Entgegen der bisherigen Annahmen zeigte die Mutation jedoch keinen signifikanten Einfluss auf die ATP- und Laktatkonzentration. Die Ergebnisse deuten darauf hin, dass FRET-sensoren grundsätzlich geeignet sind, um eine Aussage über Stoffwechselvorgänge in Motoneuronen zu treffen. Es ist jedoch möglich, dass die Anzahl der analysierten Zellen zu gering war, um einen signifikanten Unterschied nachzuweisen. Weitere Studien sind notwendig um zu untersuchen, ob eine höhere Transfektionseffizienz und eine Vereinfachung des Analyseverfahrens dazu beitragen können, verlässlichere Ergebnisse zu generieren.

Summary

MFN2 is a mitochondrial protein involved in the pathogenesis of a specific subtype of the neurodegenerative disorder Charcot-Marie-Tooth (CMT). The aim of this study was to differentiate mouse embryonic stem cells to motoneurons and to use these motoneurons as a tool to investigate metabolic changes in cells overexpressing the CMT2A-related mutation $MFN2^{R94Q}$.

Differentiation to MNs was based on a differentiation module comprising three transcriptional factors responsible for neuronal development that was under the control of a Tet-on system. The results of this study have confirmed that the administration of doxycycline and the respective patterning factors to ES cells leads to the generation of postmitotic motoneurons. Neuronal identity was phenotypically confirmed by expression of common neuronal markers. I further showed that a DIO expression system under the control of a neuron specific Hb9-promoter is sufficient to induce selective overexpression of MFN2 in neuronal cells. Among the tested reagents Lipofectamine 2000 was most efficient for transfection.

The impact of mutated MFN2 on metabolic behavior, in particular on lactate and ATP levels, was monitored using FRET based genetically-encoded indicators. The successful expression of genetic indicators was confirmed by confocal microscopy. In contrast to previous suppositions, the indicators could not detect a significant difference in lactate and ATP concentration. These findings suggest that as a basic principle, FRET indicators are a suitable tool to investigate metabolic behavior in motoneurons. However the number of cells included in this analysis might have been too low to detect a significant difference in metabolism. In order to generate more reliable results it might be necessary to further improve transfection efficiency and to establish a method that allows the easy analysis of a larger number of cells.

Abbreviations

AAV	adeno-associated virus
att	attachment site
BCA assay	bicinchoninic acid assay
bFGF	basic fibroblast growth factor
bp	base pair
cDNA	complementary DNA
CFP	cyan fluorescent protein
CMT	Charcot-Marie-Tooth disease
DAPI	4′,6-diamidino-2-phenylindole
DEST	destination vector in gateway cloning
DIO	double-floxed inverted orientation
DMEM	Dulbecco's modified eagle medium
DMSO	dimethyl sulfoxide
DNA	deoxyribonucleic acid
DNase	deoxyribonuclease
dNTP	deoxynucleotidetriphosphate
DOX	doxycycline
E. coli	*Escherichia coli*
EB	embryoid bodies
EDTA	ethylenediaminetetraacetic acid
EGF	epidermal growth factor
et al.	et alii
FCS	fetal calf serum
gapdh	glyceraldehyde 3-phosphate dehydrogenase
Gdap1	Ganglioside-induced differentiation-associated protein-1
GOI	gene of interest
HEK cells	human embryonic kidney cells
HR	heptad repeat
IB	immunoblot
ICC	immunocytochemistry
IMM	inner mitochondrial membrane
IMS	intermembrane space

iNIL-mESC	inducible mouse embryonic stem cells containing NIL transcription factors
iPS cells	induced pluripotent stem cells
IRES	internal ribosomal entry site
Isl1	islet-1
kb	kilo base pair(s)
KSR	knockout serum replacement
LB	lysogeny broth
Lhx3	LIM/homeobox protein 3
LIF	leukemia inhibitory factor
MEF	mouse embryonic fibroblast(s)
MEM	minimal essential medium
mESC	murine embryonic stem cell
MFN	mitofusin
mmc	mitomycin C
mmcMEF	mitomycin c-inactivated mouse embryonic fibroblasts
MN	motoneuron
mNCV	motor nerve conduction velocity
mtDNA	mitochondrial DNA
NEAA	non-essential amino acids
Ngn2	neurogenin 2
NLS	nuclear localisation signal
NPC	neuronal progenitor cell
OMM	outer mitochondrial membrane
Opa1	optical atrophy 1
OXPHOS	oxidative phosphorylation
P/S	penicillin/streptomycin
PBS	phosphate-buffered saline
PCR	polymerase chain reaction
PFA	paraformaldehyde
PI	propidium iodide
PVDF	polyvinylidene difluoride
RA	retinoic acid

RFP	red fluorescent protein
RIPA buffer	radioimmunoprecipitation assay buffer
RNA	ribonucleic acid
RNase	ribonuclease
rpm	rounds per minute
RT	reverse transcription
RT-PCR	real-time PCR
SC	stem cell
SDS	sodium dodecyl sulfate
SDS -PAGE	sodium dodecyl sulfate polyacrylamide gel electrophoresis
Shh	sonic hedgehog pathway
Smo	smoothened agonist of hedgehog pathway
SOC	super optimal broth with added glucose
TAE	tris-acetate-EDTA
TBS	tris-buffered saline
TE buffer	tris-EDTA buffer
TFP	teal fluorescent protein
TM	transmembrane
Tween	polyoxyethylenesorbitan monolaurate
U	enzyme unit
UV	ultraviolet

List of Figures

List of Tables

1 Introduction

Mutations in the mitochondrial protein Mitofusin 2 cause a specific subtype of the Charcot-Marie-Tooth disease (Zuchner et al., 2004).

The objective of this study was to establish a tool to evaluate metabolic alterations caused by the CMT2A-related mutation MFN2^{R94Q} in motoneurons (MNs). I therefore wanted to differentiate mouse embryonic stem cells (mESCs) to motoneurons and characterize the neuronal identity by immunocytochemistry. I further wanted to establish a transfection strategy for the selective overexpression of MFN2 in motoneurons. Finally, I aimed to study the potential metabolic alterations in neurons overexpressing mutant MFN2 compared to the wild type (wt).

1.1 Dissecting Mitochondrial Dynamics: The Mitochondrial Fusion and Fission Machinery

Mitochondria are essential for cell survival, as they are the major source of energy production in most cells. But they also fulfill additional functions such as regulating cellular metabolism and calcium homeostasis as well as induction of apoptosis (Murgia et al., 2009; Lee et al., 2004). First interest in the mitochondrial shape arose in the early 1950-ies. Electron microscope studies conducted by George E. Palade found the single mitochondrion to consist of a matrix surrounded by a double membrane with the inner membrane forming internal ridges, termed cristae mitochondriales (Palade, 1953). Palade understood mitochondria as static organelles. However, in the following decades it became evident, that mitochondria are constantly changing their shape and subcellular distribution (Bereiter-Hahn and Vöth, 1994). Today, it is generally accepted that the entity of mitochondria in one cell is a highly dynamic system that continuously reshapes in order to adapt to changing cellular demands (Schon and Przedborski, 2011). Seen from a binary point of view the entirety of mitochondria can either consist of a conglomerate of morphologically distinct small organelles or of a large interconnected network (Bereiter-Hahn, 1990).

Morphological changes in mitochondria are conducted by tightly regulated rates of fusion and fission (Sesaki and Jensen, 1999). Gaining insights into the molecular mechanism of mitochondrial fusion and fission started with the identification of the mitochondrial fusion protein Fzo in Drosophila (Hales and Fuller, 1997). In the following years, several orthologous proteins in yeast and mammals were

discovered. Today we know that at least two distinct sets of proteins govern mitochondrial dynamics: The mitochondrial fusion and fission machinery. The fusion process is a multistep mechanism consisting of coordinated fusion of the inner and outer mitochondrial membrane (IMM, OMM) and is orchestrated by three large GTPases (Song et al., 2009). As demonstrated in figure 1, Mitofusins 1 and 2 are located at the OMM and are responsible for the fusion of the outer membranes of two adjacent mitochondria (Santel and Fuller, 2001; Chen et al., 2003). This tethering step is dependent on GTP hydrolysis (Santel, 2006). Finally the dynamin family GTPase Opa1, located in the intermembrane space (IMS), mediates fusion of the inner membranes (Meeusen et al., 2006). The opposed process of mitochondrial fission is governed by the dynamin-related protein Drp1 in collaboration with several other proteins such as Fis1 and Mff (Smirnova et al., 2001; James et al., 2003; Gandre-Babbe and van der Bliek, 2008). To initiate mitochondrial fission, cytosolic Drp1 is recruited to certain spots on the mitochondrion where it forms multimeric spirals around the organelle. GTP-dependent constriction results in fission of the double membrane (Mears et al., 2011).

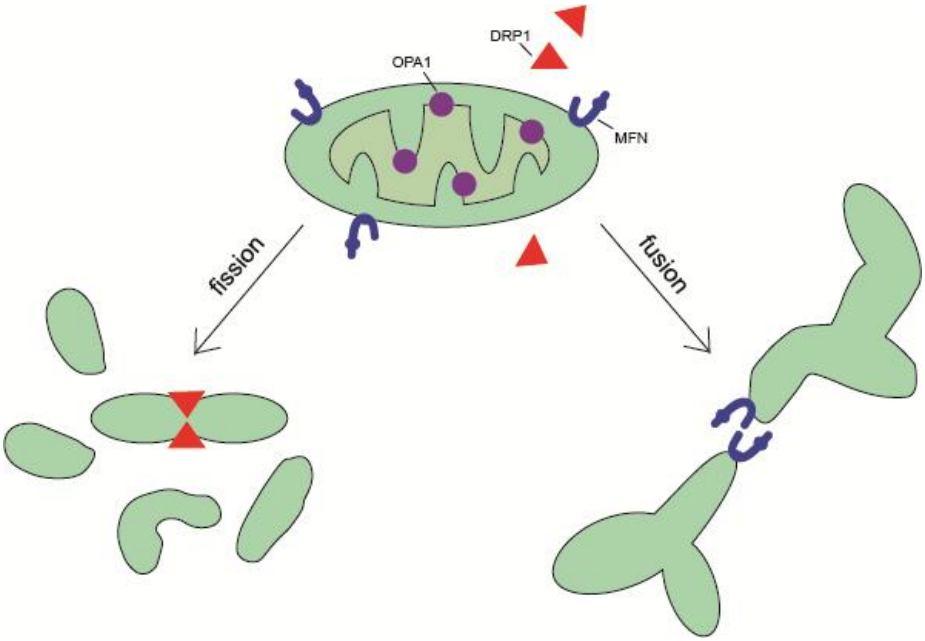

Figure 1: The mitochondrial fusion and fission machinery consists of several proteins.
Mitochondrial fusion is conducted by two proteins called Mitofusin 1 and Mitofusin 2 (MFN). They mediate fusion of the outer membranes of two adjacent mitochondria. The inner mitochondrial membrane protein Opa1 is responsible for the fusion of the inner layers of the membrane. Fission of one mitochondrion is mainly conducted by the cytosolic protein Drp1 which forms spirals around the organelle and separates it into two mitochondria. Figure adapted from Chen and Chan, 2006.

1.2 Involvement of Mitochondrial Fusion in Cellular Processes

Shaping of the mitochondrial network in response to changes of the surrounding conditions might be the most obvious function of mitochondrial fusion. In a metabolically and respiratory active cell, a system of interconnected mitochondria is predominant, whereas small and fragmented mitochondria are prevailing in quiescent and respiratory inactive cells (Westermann, 2012). Over the last decades, however, research has not ceased to broaden our horizon regarding the numerous additional functions of mitochondrial dynamics.

One purpose of mitochondrial fusion is to maintain mitochondrial functionality during the aging process. In aged cells, mitochondria are more prone to suffer from DNA lesions. This leads to coexistence of wild type and mutated mitochondrial DNA (mtDNA), a state called heteroplasmy. Considering that all mitochondrial DNA codes for proteins involved in oxidative phosphorylation (OXPHOS), it follows that accumulation of mutated mitochondrial DNA can lead to impaired respiratory capacity. Since the fusion process involves mixing of genetic material and mitochondrial matrix content, it can supply a mitochondrion containing mutated mitochondrial DNA with an intact allele from an adjacent organelle. Thereby, intermitochondrial complementation compensates for mutated mtDNA and prevents the expression of defective respiratory subunits. This process is essential to restore respiratory activity and to avoid mitochondrial dysfunction (Nakada et al., 2001; Sato et al., 2006). In the context of neurodegenerative mitochondropathies, it is important to consider that this mechanism helps to protect postmitotic cells from expressing disease phenotypes caused by mutations in the mtDNA (Santel et al., 2003).

In addition, mitochondrial fusion helps to protect the cell from stress. Mouse embryonic fibroblasts (MEFs) exposed to UV irradiation or amino acid deprivation reacted with increased mitochondrial fusion, resulting in the formation of long interconnected networks (Tondera et al., 2009). Tondera et al. referred to this phenomenon as stress- induced mitochondrial hyperfusion. They concluded that this mechanism acts as a pro-survival response against cellular stress thereby providing better mitochondrial functionality.

Furthermore, the network of highly fused mitochondria acts as an electrically connected system that allows intracellular transfer of energy to different cellular compartments.

The mitochondrial respiratory chain generates a membrane potential at sites of high oxygen concentrations, which can be transmitted along mitochondrial filaments to distinct cellular compartments with high energy demands. Impaired mitochondrial network formation due to defects in the fusion machinery can thereby affect the cellular energy supply (Skulachev, 2001). In this context it is hardly surprising that disturbance in the mitochondrial fusion process can result not only in an aberrant mitochondrial phenotype but also in severe cellular defects.

1.3 Charcot-Marie-Tooth Disease: Exploring Clinical and Genetic Aspects

One neurodegenerative disorder closely associated with disturbed mitochondrial dynamics is Charcot-Marie Tooth disease. CMT, also known as hereditary motor and sensory neuropathy, comprises a heterogeneous group of inherited peripheral neuropathies affecting motor and sensory nerves. The first description of the disease dates back to the late 19th century (Charcot and Marie, 1886; Tooth, 1886). With a prevalence of 1/2500 it is the most frequent inherited neuromuscular disorder (Skre, 1974). The common feature of all subtypes is the slowly progressive degeneration of peripheral nerves. The disorder manifests as distal muscle weakness and atrophy. Typically, weakness and atrophy start in the small muscles of the foot and in the peroneal group and continue to affect hands and forearms at a later stage. In addition, patients can suffer from distal symmetrical sensory loss and are prone to develop food deformities and diminished tendon reflexes (Harding and Thomas, 1980).

With their electrophysiology studies, Harding and Thomas largely contributed to our present classification of CMT (Harding and Thomas, 1980). Recording of motor nerve conduction velocities (mNCV) in affected individuals allows categorization in two different subtypes: A demyelinating form with a decrease in mNCV below 38 m/s and an axonal form with mNCV above 38 m/s (Harding and Thomas, 1980). Today, a revised classification that takes both electrophysiological findings and genetic aspects into account is generally accepted. This classification consists of four major groups designated as CMT 1–4. CMT1, CMT3, and CMT4 are caused by segmental de- and remyelination and onion bulb formation (demyelinating form, myelinopathy). In CMT2, loss of myelinated axons as a whole and partial regenerative sprouting is the predominant reason for the neuropathy (axonal form, axonopathy) (Kuhlenbaumer et al., 2002).

CMT2 shows great genetic heterogeneity (Harel and Lupski, 2014). Representing 20 % of all CMT2 patients, the CMT2A subtype is the most prevalent type of the axonal autosomal dominant form (Verhoeven et al., 2006). Compared to the average CMT patient, individuals affected with CMT2A show an earlier disease onset and a more severe phenotype with a high proportion of wheelchair dependency (Feely et al., 2011). CMT2A is caused by mutations in MFN2 (Zuchner et al., 2004).

1.4 Structural and Functional Aspects of Mitofusin 2

Mitofusin is a mitochondrial outer membrane protein that occurs in two homologous forms in mammals: MFN1 and MFN2 (Santel and Fuller, 2001). MFNs are evolutionary highly conserved dynamin-like GTPases mediating mitochondrial fusion. MFN1 and MFN2 are both widely expressed but show differences in tissue specific expression levels (Rojo et al., 2002). MFN1 expression is detectable in similar levels throughout various types of tissue, whereas MFN2 expression is elevated in the heart and skeletal muscle (Santel et al., 2003). Both homologues share a common molecular structure. It has previously been assumed that mammalian MFN is closely related to the yeast Fzo with the protein being anchored in the OMM by a bipartite transmembrane (TM) domain close to the C-terminal end of the protein, as shown in figure 2A. The TM domain was thought to be flanked by two hydrophobic heptad repeat domains (HR1, HR2) with a small C-terminal fragment containing HR2 and a larger N-terminal fragment containing HR1 protruding from the mitochondrion towards the cytoplasm (Santel and Fuller, 2001). The GTPase domain was located in the N-terminal half of the protein and was an integral part of the protein since GTP hydrolysis is critically required to conduct MFN dimerization and mitochondrial fusion (Santel, 2006). However, as outlined in figure 2B, Mattie et al. recently provided evidence for an alternative topology model of MFN2 (2018). While there is agreement on the structure of the N-terminal half of the protein facing the cytoplasm, they suggest that MFNs contain a single TM domain instead of a bipartite one with the C-terminal end of the protein including the HR2 domain residing in the IMS (N_{out}- C_{in} conformation) (figure 2B).

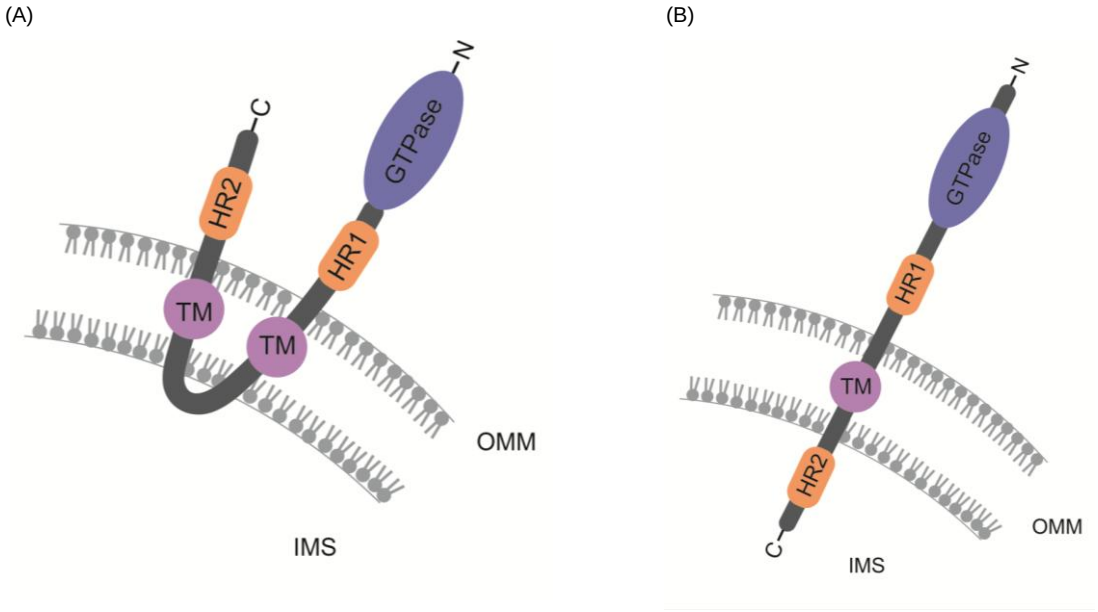

Figure 2: MFN2 is anchored in the OMM by a single TM domain rather than a bipartite one.
(A) According to previous assumptions the TM domain is a bipartite one enclosed by two heptad repeat domains (HR1, HR2). The longer N-terminal and shorter C-terminal end of the protein are protruding into the cytoplasm. The GTPase domain is located close to the N-terminal end. (B) Current topology model of MFN2 containing a single TM domain. In contrast to the previous model, the C-terminal end of the protein including the HR2 domain resides in the IMS. Figure adapted from Koshiba et al., 2004.

For mediating mitochondrial fusion, MFN1 and MFN2 can form either homotypic or heterotypic complexes. All three forms of molecular complexes are capable of promoting fusion (Chen et al., 2003). Introducing targeted null mutations in both MFN1 and MFN2 in MEF cells leads to a complete lack of mitochondrial fusion (Chen et al., 2005). In addition, MFNs play an essential role in vertebrate development. Mice devoid of either MFN1 or MFN2 die during gestation. For MFN2-deficient mice the defect was attributed to disruption of the placental trophoblast giant cell layer. The defective trophpoblast cells exhibited fragmented mitochondria consistent with a defect in mitochondrial fusion (Chen et al., 2003).

1.5 The Role of MFN2 in the Pathogenesis of Neuropathies

A conditional MFN2-knockout mouse model bypassing developmental lethality, allows the evaluation of MFN2-deficiency in adult mice (Chen et al., 2007). These mice are born clinically unremarkable but start to develop defects in balance and movement after birth. All pubs die within three weeks post partum. Consistent with movement defects, they show a reduction in cerebellar size. Chen et al. attributed the size reduction to a degenerative process rather than a lack of development. Furthermore, MFN2-null cerebella are characterized by a significant degeneration of Purkinje cells with reduction in dendritic outgrowth and spine formation. Closer

dissection of Purkinje cells showed a lack of mitochondria in dendritic tracts as well as a reduction in fusion activity (Chen et al., 2007).

The role of MFN2 mutations in axonal degeneration has been discussed controversially. Disruption of axonal transport is one potential mechanism contributing to axonopathy in mitochondrial diseases. As main supplier of energy the presence of mitochondria is critical at sites of high energy demand like synapses. A transport defect deprives neuronal cells from energy at these critical sites (Verstreken et al., 2005; Li et al., 2004). Expression of CMT2A-associated MFN2 mutants in cultured dorsal root ganglion neurons induced a severe disruption of axonal mitochondrial transport and led to abnormal clustering of small fragmented mitochondria in the proximal segments. The respective mitochondria showed a loss of fast persistent movement and an increase in time spent stationary (Baloh et al., 2007). Overexpression of MFN2 with these mutations in motoneurons of transgenic mice confirmed abnormal axonal distribution with a depletion of mitochondria in axons (Detmer et al., 2008).

All these data suggest a direct correlation between MFN2 and mitochondrial transport. Misko et al. discovered that mitochondria are associated with Kinesin motor proteins during axonal transport through interaction of MFN1 and MFN2 with the adaptor proteins Miro and Milton (2010). As a consequence, loss of MFN2 or expression of MFN2 disease mutants specifically disrupted axonal mitochondrial transport. Knockdown of the fusion protein Opa1 did not induce a transport defect, indicating a fusion-independent role of MFN2 in mitochondrial transport (Misko et al., 2010). Because of high energy demands at cellular compartments distant from the soma neurons are particularly dependent on effective axonal transport of mitochondria. In patients suffering from CMT2A a highly specific type of neuronal cells is affected: Spinal motor neurons and dorsal root ganglion sensory neurons (Cartoni and Martinou, 2009). Considering that peripheral sensory and motor axons are the longest in the body, it is hardly surprising that they are the most sensitive to defects in mitochondrial transport (Baloh et al., 2007).

On closer inspection, the knockdown of MFN does not only impair mitochondrial transport but also leads to severe mitochondrial and cellular dysfunction. Cells deficient for both MFNs show a loss of mitochondrial membrane potential, impairment in mitochondrial respiratory capacity and reduced cell proliferation. In the absence of

either one of the homologues, fusion levels are still reduced but all of the cellular functions mentioned above remain unchanged. These findings indicate that one MFN isoform is sufficient to prevent major cellular dysfunction (Chen et al., 2005).

1.6 Mutated MFN2 Causes Charcot-Marie-Tooth 2A

As previously mentioned, CMT2A is caused by mutations in MFN2 (Zuchner et al., 2004). About 60 different MFN2 mutations have been reported in CMT2A patients. The majority of these mutations are single point mutations leading to an amino acid substitution. One of the most common mutations affects the amino acid residue at position 94 ($MFN2^{R94Q}$), which is located within the GTPase domain (Cartoni and Martinou, 2009).

A transgenic mouse model carrying the $MFN2^{R94Q}$ mutation showed a classical CMT phenotype with locomotor impairment, confirming the causative role of mutated MFN2 for the development of CMT (Cartoni et al., 2010). The CMT phenotype was accompanied by distal accumulation of mitochondria in the sciatic nerve (Cartoni et al., 2010) and defects in complex II and V of the mitochondrial respiratory chain leading to a decrease in mitochondrial ATP production (Guillet et al., 2011). Recent studies in $MFN2^{R94Q}$ mice showed that mitochondria are incapable to adequately increase ATP production upon axonal activity, presumably due to decoupling of ATP and reactive oxygen species production (van Hameren et al., 2019). This assumption was corroborated by experiments in $MFN2^{R94Q}$ expressing MEF cells. Mild oxidative stress in these cells leads to an increase in mitochondrial respiration but fails to increase ATP production accordingly thereby providing further evidence for an uncoupling of respiration and ATP production (Wolf et al., 2019).

MFN-null cells exogenously overexpressing $MFN2^{R94Q}$ lacked any mitochondrial fusion activity, suggesting that $MFN2^{R94Q}$–$MFN2^{R94Q}$ homocomplexes are incapable of accomplishing mitochondrial fusion. The presence of endogenous MFN1 however, enabled the formation of heterooligomeric $MFN1^{wt}$- $MFN2^{R94Q}$ complexes and led to rescue of fusion activity (Detmer and Chan, 2007). These results indicate that in the presence of endogenous wild type MFN1, $MFN2^{R94Q}$ is functional. In this respect the wide expression pattern of MFN1 might act as a protecting mechanism, preserving mitochondrial fusion in CMT2A patients carrying mutated MFN2 alleles (Santel et al., 2003). Tissues with low endogenous MFN1 expression are therefore more vulnerable to defects in MFN2. A low expression level of endogenous MFN1 in peripheral

nerves could be a possible explanation for their specific susceptibility to damage in mitochondrial proteins (Detmer and Chan, 2007).

1.7 Characterization of Stem Cells

To study the role of MFN2 in CMT and in neuronal metabolism *in vitro*, a suitable model is required. Neural tissue of diseased individuals best recapitulates the properties of neuronal cells *in vivo* but can potentially harm the patient during the biopsy procedure. Moreover, apart from legal and ethical barriers, human primary neurons are difficult to culture. One way to circumvent both obstacles is to differentiate motoneurons from stem cells *in vitro*. Stem cells are commonly defined as undifferentiated cells with the capacity for long-term self-renewal and the ability to differentiate into specialized cell types (Rippon and Bishop, 2004). During embryogenesis, all kinds of tissues and ultimately organs arise from stem cells which emphasizes their critical importance. In the adult, a certain number of tissue-specific stem cells persists in several niches throughout the body, e.g. in the bone marrow, brain, liver and skin, where they provide the capacity for replacement of differentiated cells (Wagers et al., 2002).

For *in vitro* studies murine embryonic stem cells are most commonly used. The cells are derived from the inner cell mass of a pre-implantation blastocyst. In the natural course of events, the inner cell mass would form the murine embryo and therefore has the property to develop into all sorts of tissue. Since these cells are rather short-lived, addition of leukemia inhibitory factor (LIF) to mESCs or growth on a feeder layer of murine embryonic fibroblasts is necessary to enable unlimited cultivation in an undifferentiated state (Williams et al., 1988). Withdrawal of LIF or the feeder layer and switching to culturing in suspension conditions allows spontaneous differentiation, phenotypically indicated by formation of aggregates termed embryoid bodies (EBs) (Keller, 1995). These spherical cell clusters resemble post-implantation embryonic tissue and contain derivates of all three germ layers (Abe et al., 1996). Returning of EBs to adherent culture conditions allows differentiation to mature somatic cell types when induced with the respective signals.

Since the first description of murine embryonic stem cells in the early eighties of the last century, stem cell research achieved a great deal (Evans and Kaufman, 1981; Martin, 1981; Lu et al., 2014). With the help of ESCs we were able to investigate the early stages of mammalian development *in vitro* and to generate a wide range of

transgenic animals. To date we have accomplished to derive a variety of human ESCs from spare embryos of *in vitro* fertilization (Thomson, 1998; Mitalipova et al., 2003).

1.8 Directed Differentiation of Stem Cells to Motoneurons

Differentiation of stem cells to mature somatic cells requires induction with appropriate signals. For *in vitro* differentiation to neuronal cells, signals that recapitulate the natural development processes during neurogenesis are necessary (Wichterle et al., 2002). The development of the nervous system *in vivo* originates from progenitor cells in the neural tube. Their position within the neural tube and thus the concentration of inductive signals to which the progenitor cell is exposed determines its identity. Ultimately, the progenitor cell is allocated to a specific cell fate, thereby establishing a variety of different central nervous system neural subtypes. The fate of the differentiating cells is determined by two different signaling systems. Specification along the rostrocaudal axis of the neural tube is induced by retinoic acid (RA) and establishes the main subdivisions of the central nervous system. Within each of these subdivisions, cell type specification along a dorsoventral axis is mediated by agonists of the sonic hedgehog (Shh) pathway (Jessell, 2000).

Wichterle et al. translated these insights into a differentiation protocol for the generation of spinal motoneurons. In this protocol, administration of RA to EBs leads to generation of neuronal progenitor cells with spinal cord characteristics. Further exposure of these cells to Shh establishes an expression profile consistent with postmitotic spinal motoneurons (Wichterle et al., 2002).

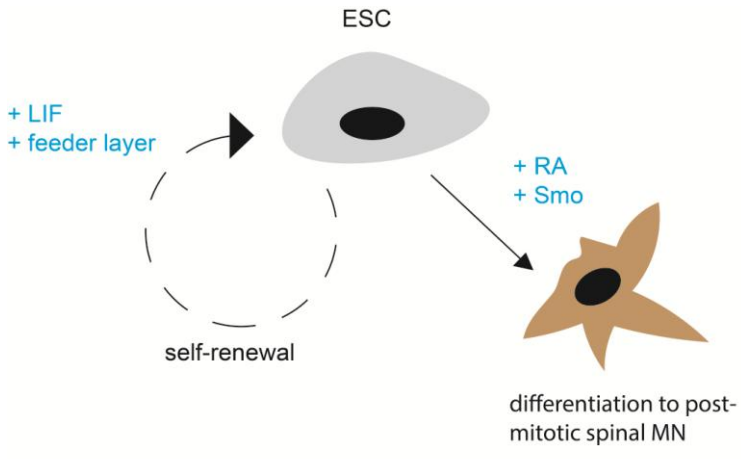

Figure 3: Depending on the surrounding factors, embryonic stem cell can adopt different courses.
Depending on culture conditions and the presence of chemical mediators a stem cell can embark on two paths *in vitro*. For maintenance and propagation, ESCs are cultured on a feeder layer of MEF cells in the presence of LIF. Differentiation to MNs is induced by addition of retinoic acid and Smo, an agonist of the the sonic hedgehog pathway. Figure adapted from Smith, 2001.

Since the differentiation of spinal MNs from human ES cells using conventional differentiation protocols is a time intensive process with a low MN yield, studies that require a certain number of cells cannot be performed. Hester et al. helped resolving this problem by identifying rate limiting factors in the neuronal differentiation process *in vitro* (Hester et al., 2011). They found that viral transduction of the three transcriptional factors Neurogenin 2 (Ngn2), Islet-1 (Isl1), and LIM/homeobox protein 3 (Lhx3) (NIL-factors) in differentiating motoneurons accelerated the differentiation process from previously 60 days to 11 days and increased the efficiency from 10-40 % to 60- 70 %.

Mazzoni et al. then implemented a sophisticated differentiation strategy in mouse ES cells based on stable overexpression of the NIL-factors under control of a "Tet-On"-system (iNIL-ES cells). As depicted in figure 4, iNIL-ES cells contain a doxycycline inducible polycistronic expression construct consisting of the open reading frames for Ngn2, Isl1 and Lhx3. First, iNIL-ES cells are treated with RA and Shh pathway agonists to stimulate basic neuronal differentiation. Subsequenty, induction of NIL-factors expression is achieved by doxycyclin administration. Culturing of induced cells for 7-10 days is sufficient to generate postmitotic MN identity with mature electrophysiological properties (Mazzoni et al., 2013). By developing a cell line that is comparatively easy to culture over a long period of time and that offers an individual starting point for differentiation upon doxycyline treatment, Mazzoni et al. provided cell biologists with a valuable and efficient technique to quickly generate a large number of spinal motoneurons. These differentiated motoneurons are particularily suitable to assess mitochondrial behavior in neuronal cells and are therefore used as model for studies in this work.

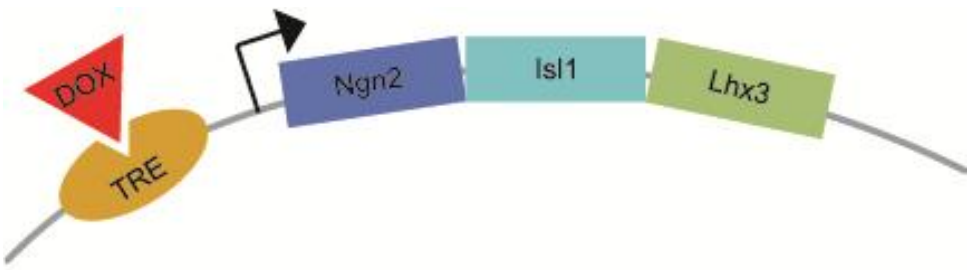

Figure 4: Three transcriptional factors form the NIL programming module.
The Doxycyclin-inducible expression module consists of the transcriptional factors Neurogenin 2 (Ngn2), Islet-1 (Isl1), and LIM/homeobox protein 3 (Lhx3). Expression is activated in the presence of doxycyclin (DOX). Doxycylin binds to the tetracycline response element (TRE) and enables expression of the downstream elements. Ultimately expression of NIL-factors results in rapid and efficient specification to spinal motoneurons. Figure adapted from Mazzoni et al., 2013.

2 Materials

2.1 Materials for Cell Culture and Biochemical Methods

Cell Culture Media and Supplements

Product	Company
0.05 % Trypsin-EDTA	Life-Technologies, Carlsbad, USA
Advanced DMEM/F-12 (Dulbecco's Modified Eagle Medium/Ham's F-12)	Gibco-Life Technologies, Carlsbad, USA
Ampicillin Sodium Salt	Sigma-Aldrich, St Louis, USA
Biotase	Biochrom, Berlin, Germany
Doxycycline	Sigma-Aldrich, St Louis, USA
Dulbecco's Modified Eagle Medium (DMEM)	Thermo Fisher Scientific, Waltham, USA
Dulbecco's Phosphate-Buffered Saline (PBS)	Sigma-Aldrich, St Louis, USA
EmbryoMax® ES DMEM	Merck Millipore, Billerica, USA
Epidermal Growth Factor (EGF)	Sigma-Aldrich, St Louis, USA
ESGRO R mLIF Medium Supplement	Merck Millipore, Billerica, USA
FGF-Basic Recombinant Human Protein	Thermo Fisher Scientific, Waltham, USA
HyClone Fetal Bovine Serum	Thermo Fisher Scientific, Waltham, USA
Kanamycin Sulfate	Sigma-Aldrich, St Louis, USA
KnockOut™ Serum Replacement	Invitrogen, Carlsbad, USA
Laminin L2020	Sigma-Aldrich, St Louis, USA
L-Cystein	Sigma-Aldrich, St Louis, USA
Leukemia Inhibitory Factor (LIF)	Merck Millipore, Billerica, USA
L-Glutamine (200 mM)	Life Technologies, Carlsbad, USA
MEM Non-Essential Amino Acids	Life Technologies, Carlsbad, USA
Mitomycin-C	Sigma-Aldrich, St Louis, USA
N2 Supplement	Gibco-Life Technologies, Carlsbad, USA
Neurobasal Medium	Gibco-Life Technologies, Carlsbad, USA
Opti-MEM® I Reduced Serum Medium	Gibco-Life Technologies, Carlsbad, USA

Product	Company
Penicillin-Streptomycin solution (10000 U/ml penicillin, 10 mg/ml streptomycin)	Sigma-Aldrich, St Louis, USA
Poly-L-Lysine solution	Sigma-Aldrich, St Louis, USA
Propidium Iodide	Sigma-Aldrich, St Louis, USA
Recombinant Human FGF-Basic	BioSource International, Camarillo, USA
Retinoic Acid	Sigma-Aldrich, St Louis, USA
Sodium Pyruvate	Gibco-Life Technologies, Carlsbad, USA

Table 1: Cell Culture Media and Supplements

Transfection Reagents

Reagent	Company
Effectene Transfection Reagent	Quiagen, Dusseldorf, Germany
Lipofectamine 2000	Invitrogen, Carlsbad, USA
Lipofectamine 3000	Invitrogen, Carlsbad, USA

Table 2: Transfection Reagents

Cell Lines

Cell Line	Characteristics	Source
HT22	mouse hippocampal cell line	Davis and Maher, 1994
mES-iNIL	mouse ES cells enclosing the NIL transcription factors (Ngn2, Isl1 and Lhx3) driven by a doxycycline inducible promoter	Kindly gifted from Esteban O. Mazzoni, New York, USA
mES-MN	motoneurons differentiated from mES-iNIL cells	generated in this work
mNPC	neural progenitor cells differentiated from mES-iNIL cells	generated in the lab according to Fazeli et al., 2013
mNPC-MN	motoneurons differentiated from mNPC	generated in this work

Table 3: Cell Lines

Antibodies and Dyes

Primary Antibody/ Dye	Purpose	Host Species	Dilution	Company
anti-GAPDH (14C10)	IB	rabbit monoclonal	1/4000	Cell Signaling Technology, Cambridge, United Kingdom
anti- Neuron-Specific β-III Tubulin (MAB1195)	IB	mouse monoclonal	1/1000	R&D Systems, Minneapolis, USA
Acti-stain 670 phalloidin	ICC			Cytoskeleton, Denver, USA
anti-Islet 1/2 (39.4D5-s)	ICC	mouse monoclonal	undiluted	Developmental Studies Hybridoma Bank
anti-Hb9 (81.5C10-c)	ICC	mouse monoclonal	1/100	Developmental Studies Hybridoma Bank
anti-Mitofusin 2 (N153/5)	ICC	mouse monoclonal	1/200	UC Davis/NIH NeuroMab Facility, Davis, USA
anti-mouseHb9	ICC	rabbit monoclonal	1/100	Kind gift from the Jessel lab
anti-RFP (5F8)	ICC	rat	1/1000	Chromotek, New York, USA
anti-β3-Tubulin (D71G9)	ICC	rabbit	1/200	Cell Signaling Technology, Cambridge, United Kingdom
DAPI (4',6-Diamidino-2-Phenylindole, dilactate)	ICC			Life Technologies, Carlsbad, USA

Table 4: Primary Antibodies and Dyes

Secondary Antibody	Purpose	Host Species	Dilution	Company
anti-Mouse IgG (H+L), Alexa FluorR 488	ICC	goat	1/500	Thermo Fisher Scientific, Waltham, USA
anti-Rabbit IgG (H+L), Alexa FluorR 488	ICC	goat	1/500	Thermo Fisher Scientific, Waltham, USA
anti-Rabbit IgG (H+L), DyLight 680	IB	goat	1/15000	Cell Signaling Technology, Cambridge, United Kingdom

Table 5: Secondary Antibodies

2.2 Materials for Molecular Biological Methods

Chemicals

Product	Company
1 kb Plus DNA Ladder	Thermo Fisher Scientific, Waltham, USA
2-Mercaptoethanol (50 mM)	Thermo Fisher Scientific, Waltham, USA
Agarose Basic	AppliChem, Darmstadt, Germany
cOmplete™ Mini Protease Inhibitor Cocktail	Sigma-Aldrich, St Louis, USA
Dimethyl Sulfoxide (DMSO)	Sigma-Aldrich, St Louis, USA
Ethanol ROTIPURAN® ≥ 99.8 %	Carl Roth, Karlsruhe, Germany
Fluorescence Mounting Medium	Dako, Carpinteria, USA
Glycerol	Sigma-Aldrich, St Louis, USA
iQ™ SYBR Green Supermix	Bio-Rad Laboratories, Hercules, USA
L-Cystein	Sigma-Aldrich, St Louis, USA
MagicMark™ XP Western Protein Standard	Thermo Fisher Scientific, Waltham, USA
Midori Green Advance	NIPPON Genetics Europe, Düren, Germany
Nuclease-free Water	Life-Technologies, Carlsbad, USA
Ponceau S solution	Sigma-Aldrich, St Louis, USA
Powdered Milk	Carl Roth, Karlsruhe, Germany
Roti®-Histofix 4 %	Carl Roth, Karlsruhe, Germany
Roti®-ImmunoBlock	Carl Roth, Karlsruhe, Germany
Triton™ X-100	Sigma-Aldrich, St Louis, USA
Trypan Blue Solution	Invitrogen, Carlsbad, USA
TWEEN® 20	Sigma-Aldrich, St Louis , USA

Table 6: Chemicals

Media

Medium	Company
LB-Agar, powder	**Invitrogen, Carlsbad, USA**
LB-Broth Base (LB medium)	**Invitrogen, Carlsbad, USA**
S.O.C. Medium	**Invitrogen, Carlsbad, USA**

Table 7: Media

Buffers

Buffer	Company
10x Tris/Glycine/SDS Running Buffer	Bio-Rad Laboratories, Hercules, USA
4x LDS Sample Buffer	Thermo Fisher Scientific, Waltham, USA
BlueJuice™ Gel Loading Buffer	Thermo Fisher Scientific, Waltham, USA
Pierce RIPA-Buffer	Thermo Fisher Scientific, Waltham, USA

Table 8: Buffers

Self-made Buffer	Ingredients
FACS Buffer	0.5 % BSA in PBS (+)
TAE Buffer (50x)	**2 M tris base** **1 M acetic acid** **0.05 M EDTA (pH 8)**
TE Buffer	**10 mM Tris (pH 8.0)** **1 mM EDTA**

Table 9: Self-made Buffers

Enzymes

All restriction enzymes were purchased from New England Biolabs (Ipswich, USA) or Thermo Fisher Scientific (Waltham, USA) and used with the respective buffer.

Other Enzymes	Company
DNase	Invitrogen, Carlsbad, USA
Gateway® LR Clonase® II Enzyme Mix	Invitrogen, Carlsbad, USA
Proteinase K	Quiagen, Dusseldorf, Germany
T4 DNA Ligase	New England Biolabs, Ipswich, USA

Table 10: Enzymes

Plasmids

Plasmid	Description	Source
pENTR6C-MFN2(WT)	MFN2 (WT) in entry vector	generated in the laboratory
pENTR6C-MFN2(R94Q)	MFN2 (R94Q) in entry vector	generated in this work
pENTR6C-MFN2(K109A)	MFN2 (K109A) in entry vector	generated in the laboratory
pENTR5B-AT1.03^{YEMK}	AT1.03^{YEMK} (ATP indicator) in entry vector	generated in the laboratory
pENTR2B-(MCS Perc Avi HA)-Laconic	Laconic (lactate indicator) in entry vector	generated in the laboratory
pPB-CAG::HA	empty piggyBac destination vector	generated in the laboratory
pPB-CAG::HA- AT1.03^{YEMK}	AT1.03^{YEMK} in piggyBac vector	generated in this work
pPB-CAG::HA- Laconic-	Laconic in piggyBac vector	generated in this work
pAAV-EF1a::DIO-HA-DEST-IRES-mcherry-NLS	empty DIO construct in pAAV vector encoding nuclear mCherry	Prof. Albrecht Stroh, Johannes Gutenberg University Mainz, Germany
pAAV-EF1a::DIO-HA-MFN2(WT)-DEST-IRES-mcherry-NLS	DIO construct with MFN2 (WT)	generated in this work
pAAV-EF1a:: DIO-HA-MFN2(R94Q)-DEST-IRES-mcherry-NLS	DIO construct with mutated MFN2 (R94Q)	generated in this work
pAAV-EF1a:: DIO-HA-MFN2(K109A)-DEST-IRES-mcherry-NLS	DIO construct with mutated MFN2 (K109A)	generated in this work
pAAV-mHb9-miniCMV::Cre	Cre recombinase under control of a mouse Hb9 promoter	generated in the laboratory

Plasmid	Description	Source
CAG::Cre	Cre recombinase under control of a common CAG promoter	generated in the laboratory
pPB-CAG::HA-IRES-VENUS-DEST	yellow fluorescent protein VENUS	generated in the laboratory

Table 11: Plasmids

Bacteria

Bacterial Strain	Genotype	Company
DH5α™	**F– Φ80lacZΔM15 Δ(lacZYA-argF) U169 recA1 endA1 hsdR17 (rK–, mK+) phoA supE44 λ– thi-1 gyrA96 relA1**	**Invitrogen, Carlsbad, USA**
One Shot® *ccd*B Survival™ 2 T1^{R} Competent Cells	**F-mcrA Δ(mrr-hsdRMS-mcrBC) Φ80lacZΔM15 ΔlacX74 recA1 araΔ139 Δ(ara-leu)7697 galU galK rpsL (StrR) endA1 nupG fhuA::IS2**	**Invitrogen, Carlsbad, USA**

Table 12: Bacteria

Primers

Primers were designed using Beacon Designer.

Primer	Sequence (5’ →3’)	Length (bp)	Melting Temperature (°C)
MFN2-fwd	TGAGCACACCTACAGAGA	18	61
MFN2-rev	GCCAAACGCAAGATACAAG	19	61.4
β-actin-fwd	AATCTTCCGCCTTAATACT	19	58.8
β-actin-rev	AGCCTTCATACATCAAGT	18	58.4

Table 13: Primers

Kits

Kit	Company
BC Assay Protein Quantitation Kit	Interchim, Montluçon, France
Gibson Assembly Cloning Kit	New England Biolabs, Ipswich, USA
Herculase II Fusion Enzyme with dNTP combo	Agilent Technologies, Santa Clara, USA
High Capacity cDNA Reverse Transcription Kit	Thermo Fisher Scientific, Waltham, USA
NucleoBond® Xtra Maxi	MACHEREY-NAGEL, Düren, Germany
ZR RNA MiniPrep™	Zymo Research, Irvine, USA
Zymoclean™ Gel DNA Recovery Kit	Zymo Research, Irvine, USA
Zyppy™ Plasmid Miniprep Kit	Zymo Research, Irvine, USA

Table 14: Kits

Labware

Material	Company
µ-Slide 8-Well Glass Bottom	ibidi, München, Germany
4-15 % Mini-PROTEAN® TGX Stain-Free™ Precast Gels	Bio-Rad Laboratories, Hercules, USA
Falcon™ Cell Strainer 70 µl	Thermo Fisher Scientific, Waltham, USA
Trans-Blot® Turbo™ Mini PVDF Transfer	Bio-Rad Laboratories, Hercules, USA

Table 15: Labware

Instruments

Device	Company
Agarose Electrophoresis System	Bio-Rad Laboratories, Hercules, USA
BD FACS CantoTM II	BD Biosciences, Franklin Lakes, USA
BX51 Fluorescence Microscope	Olympus, Tokio, Japan
Centrifuge 5430	Eppendorf, Hamburg, Germany
CFX Connect™ Real-Time PCR Detection System	Bio-Rad Laboratories, Hercules, USA
CO_2-Inkubator MCO-20AIC	Sanyo, Moriguchi, Japan
Fresco 21 Centrifuge Heraeus	Thermo Fisher Scientific, Waltham, USA
Heratherm Incubator	Thermo Fisher Scientific, Waltham, USA
Microscope Motic AE20	Motic, Hong Kong, China
Mini-PROTEAN® Tetra Cell electrophoresis system	Bio-Rad Laboratories, Hercules, USA
MSC-Advantage Sterile Bench	Thermo Fisher Scientific, Waltham, USA
Multifuge 3 L-R Zentrifuge Heraeus	Thermo Fisher Scientific, Waltham, USA
Nanodrop 2000c	Peqlab, Erlangen, Germany.
Neubauer-improved Counting Chamber	Paul Marienfeld, Lauda-Königshofen, Germany
Odyssey® Sa Infrared Imaging System	LI-COR, Lincoln, USA
PowerPac Basic Power Supply	Bio-Rad Laboratories, Hercules, USA
TCS SP5 confocal microscope	Leica Microsystems, Wetzlar, Germany
Tecan Reader Infinite M200 Pro	Tecan Group, Zurich, Switzerland
Thermomixer F 1.5	Eppendorf, Hamburg, Germany
Trans-Blot Turbo Transfer System	Bio-Rad Laboratories, Hercules, USA
Vacuum Pump, VACUSAFE	Integra-Biosciences, Zizers, Switzerland
Water bath, LAUDA Aqualine AL 12	LAUDA, Delran, USA

Table 16: Instruments

Software

Program	Company
Adobe Illustrator CS6	Adobe Systems, San Jose, USA
Adobe Photoshop	Adobe Systems, San Jose, USA
Beacon Designer	PREMIER Biosoft, Palo Alto, USA
FACSDiva™ Software	BD Biosciences, Franklin Lakes, USA
FlowJo 8.7.3	Tree Star, Ashland, USA
Graph Pad Prism 6	GraphPad Software, La Jolla, USA
i-control™ – Microplate Reader Software	Tecan Group, Zurich, Switzerland
ImageJ	National Institutes of Health, Bethesda, USA
Leica LAS AF lite	Leica Microsystems, Wetzlar, Germany
Microsoft Office	Microsoft Corporation, Redmond, USA
ODYSSEY Sa	LI-COR, Lincoln, USA

Table 17: Software

3 Methods

3.1 Methods in Cell Culture

Culturing and Passaging of Eukaryotic Cells

All eukaryotic cell lines were cultivated in 10 cm tissue culture plates with 10 ml of the respective growth medium at 37 °C and 5 % CO_2. Cells were passaged at a confluency of 80-90 %. For passaging the medium was removed and cells were carefully rinsed with PBS. Cells were incubation with 1 ml 0.05 % Trypsin-EDTA for 3-5 min at 37 °C. The reaction was terminated by addition of 9 ml of growth medium containing FCS. Cell counting was performed on an improved Neubauer Counting Chamber after staining with Trypan blue. Cells were centrifuged at 1000 rpm for 3 min, the supernatant was discarded, and fresh growth medium was added. A suitable number of cells was transferred to a new plate.

Cryoconservation and Thawing of Eukaryotic Cells

Cells were trypsinized and centrifuged at 1000 rpm for 3 min. The pellet was resuspended in an appropriate amount of freezing medium consisting of 90 % FCS and 10 % DMSO yielding a density of 3-5x10^6 cells/ml. 1 ml of cell suspension was transferred to one cryovial. The cryovials were kept in a CoolCell® freezing container at -80 °C overnight to allow gradual cooling. For long time storage the vials were kept in liquid nitrogen.

To retake cells into culture a cryovial was thawed in a 37 °C water bath. The cell suspension was transferred to 5 ml of prewarmed growth medium. After centrifugation at 1000 rpm for 3-5 min the supernatant was discarded. 10 ml of fresh growth medium were added, and cells were transferred to a 10 cm plate.

Culturing of Mouse Embryonic Stem Cells

Inducible mouse embryonic stem cells containing NIL-transcription factors (iNIL-mESC) were cultured on a layer of mitomycin c-inactivated mouse embryonic fibroblasts (mmcMEF) in EmbryoMax ES DMEM supplemented with 10 % FCS, 2 mM L-glutamine, 1 %P/S (100 U/ml penicillin with 100 µg/ml streptomycin), 100 µM 2-mercaptoethanol and 100 U/ml leucemia inhibitory factor (LIF) (ES medium). The medium was changed daily. Cells were passaged to a new layer of mmcMEF cells at a ratio of 1/10.

Differentiation of Mouse Embryonic Stem Cells to Motoneurons

3-5x10^5 cells per ml were seeded without a feeder layer in Advanced DMEM/F12 and Neurobasal medium in equal shares supplemented with 10 % Knockout Serum Replacement (KSR), 2 mM L-Glutamine, 1 % P/S and 100 µM 2-mercaptoethanol (MN medium) to initiate formation of embryoid bodies (EB). On the second day in culture (d2), the cell suspension was carefully transferred to a tube and rested for 10 min to allow settlement of EBs by gravity. The supernatant was aspirated. The EBs were resuspended in fresh MN medium and plated on a non-adhesive bacterial plate. Patterning of EBs was initiated by supplementing the medium with 1 µM all trans-retinoic acid and 0.5 µM Smo agonist of hedgehog signaling. Addition of 3 µg/ml doxycycline on d2 induced expression of the NIL-expression cassette.

On d4 cells were transferred to laminin-coated plates to induce adherence to the ground. Medium was changed on d5. Analysis of the cells was performed on d5-10.

Culturing of Neuronal Precursor Cells

Neuronal precursor cells (NPC) were cultured in DMEM-F12 medium supplemented with N_2-supplement, 100 µM non-essential amino acids (NEAA), 2 mM L-Glutamine, 1 % P/S, 100 µM 2-mercaptoethanol, 20 ng/µl epidermal growth factor (EGF) and 10 ng/µl basic fibroblast growth factor (bFGF) (NPC medium). The medium was changed daily, and cells were passaged at confluency of 80-90 % at a ratio of 1/5.

Differentiation of Neuronal Precursor Cells to Motoneurons

Differentiation was induced by seeding 0.6-1x10^5 NPCs per ml on a laminin-coated plate in MN medium. Medium was changed daily. For the first 3 d the medium was supplemented with 3 µg/ml doxycyline. Cells were analyzed on d5-10.

In case of transfection of NPCs before differentiation medium consisted of NPC medium and MN medium in equal shares on the first day after transfection. After that differentiation followed the usual protocol.

Coating of Culture Plates

Poly-L Lysine solution was diluted in PBS at a ratio of 1/7. A 6-well plate was covered with 300 µl of the solution per well and incubated at 37 °C for 1 h. After incubation the solution was aspirated, and the growth surface was rinsed with PBS. 300 µl of

laminin solution (5 µg/ml diluted in sterile water) were added per well. The plate was further incubated at 37 °C overnight. Prior to use the laminin solution was removed.

Generation of Mitomycin C Inactivated MEF Cells

MEF cells were cultured in DMEM supplemented with 10 % FCS, 2 mM L-glutamine, 1 % P/S, 1 % sodium pyruvate, 100 µM NEAA and 100 µM 2-mercaptoethanol. Cells were split at a ratio of 1/4 at 80-90 % confluency. For inactivation of cell growth, the cells were incubated with MEF medium containing 1 % mitomycin c for 2-4 h. Cells were thoroughly washed with PBS and resuspended in MEF medium enriched with 20 % FCS and 10 % DMSO. 1 ml medium containing $4x10^6$ cells was transferred to one cryovial. The cryovials were cooled at -20 °C for 1 h, followed by cooling to -80 °C overnight. For long time storage cells were kept in liquid nitrogen.

Transient Transfection of Eukaryotic Cell Lines

Transfection with plasmid DNA was performed using different reagents according to the manufacturers' instructions. Transfection with Lipofectamine 2000 will be discussed in more detail. The underlying mechanism is the formation of liposomes. Liposomes consist of lipid subunits of the reagent and negatively charged nucleic acid molecules. The cationic liposomes are able to fuse with the negatively charged plasma membrane of the cell which enables the DNA to enter the target cell.

One day prior to transfection, an appropriate number of cells was seeded in a 6- or 12-well plate to reach 60-80 % confluency. Medium was changed to growth medium free of antibiotics one hour prior to transfection. For each well in a 6-well plate 10 µl Lipofectamine 2000 and 4 µg of DNA were diluted 250 µl OptiMEM each. If more than one plasmid was used the amount of Lipofectamine remained constant and 2.5 µg of DNA were used per plasmid. After incubation for 5 min at room temperature the diluted DNA and the diluted reagent were combined. Further incubation for 20 min allowed formation of DNA-Lipofectamine complexes. After termination of this process the solution was added to the cells dropwise. The plate was returned to the incubator. Medium was changed after 4h to prevent excessive toxic effects of Lipofectamine.

If Lipofectamine 3000 was used 3 µl of Lipofectamine 3000 were diluted in 50 µl OptiMEM medium for each well in a 12-well plate. 1 µg of the plasmid was diluted in 50 µl OptiMEM medium containing 2 µl P3000 Enhancer Reagent. Diluted DNA and

diluted Lipofectamine 3000 were combined and incubated for 5 min at room temperature. Finally, the solution was added to the cells dropwise.

If Effectene was used 0.6 µg DNA and 4.8 µl Enhancer were diluted in 75 µl EC Buffer. After incubation at room temperature for 5 min 12 µl Effectene Transfection Reagent were added. Further incubation for 10 min enabled complex formation. Simultaneously cells were washed with PBS and fresh growth medium was added. After incubation the transfection solution was diluted in 400 µl of growth medium an immediately added to the cells.

Protein expression was evaluated 24-48 h after transfection by fluorescence microscopy.

3.2 Molecular Biological Methods

Transformation of Competent Bacteria

Transformation of competent Escherichia coli (*E. coli*) was performed using the heat-shock-method. 100 µl of DH5α E.coli were thawed on ice and 1 µl of the required plasmid (50-100 ng/µl) was added. Bacteria were incubated on ice for 30 min and then heat-shocked at 42 °C for 1 min. Finally, bacteria were replaced on ice for 2 min. To enable proliferation 500 µl S.O.C.-medium was added and bacteria were incubated for 60 min at 37 °C and 300 rpm. For selection cells were spread on lysogeny broth (LB) agar plates containing 100 µg/ml ampicillin or 50 µg/ml kanamycin and incubated at 37 °C overnight.

Cryoconservation of Bacterial Strains

For long time storage of bacterial strains glycerol stocks were created. 800 µl of a bacteria overnight culture were mixed with 200 µl 80 % glycerol solution and stored in a cryovial at -80 °C.

Plasmid DNA Purification

To isolate plasmid DNA from minicultures of transformed E. coli the Zyppy^{TM} Plasmid Miniprep Kit was used according to the manufacturer's instructions. Single bacteria colonies were picked from a previously incubated agar plate and grown in 2 ml LB-medium supplemented with antibiotics overnight at 37 °C and 220 rpm (minicultures). Lysis Buffer was added to1200 µl of bacteria culture and induced alcaline lysis. After terminating the reaction, the sample was centrifuged at $12x10^3$ rpm for 2 min to pellet the cell debris. The supernatant was loaded onto a spin column. A second centrifugation step was conducted to allow binding of plasmid DNA to the spin column. Finally, the column was washed twice and DNA was eluted with 30 µl of nuclease-free water. The amount of DNA was measured with a NanoDrop 2000 spectrophotometer. If larger amounts of DNA were required, the NucleoBond® Xtra Maxi Kit was used on a 200 ml overnight culture.

Agarose Gel Electrophoresis

Gel electrophoresis is a standard technique to separate DNA by size and can be used to evaluate a DNA restriction product or a polymerase chain reaction (PCR) product. Applying current to an agarose gel loaded with DNA samples leads to

migration of the negatively charged DNA towards the positive electrode. Small DNA molecules can pass the gel more quickly and will therefore migrate further. Applying the samples next to a DNA ladder allows evaluation of the size of the fragment.

Depending on the expected size of the fragments, agarose powder was dissolved in TAE buffer to generate a 0.5 %-2 % gel. For visualization of DNA under UV-light Midori Green was added 1:4x 10^4. The solution was allowed to cool in a gel tray. DNA samples were mixed with BlueJuice™ Gel Loading Buffer and loaded onto the gel alongside with a 1 kb plus DNA ladder. Electrophoresis was run at 80-150 V in TAE buffer. DNA bands were visualized under UV light at 254 nm.

Gel Extraction of DNA Fragments

To isolate DNA bands from an agarose gel the Zymoclean™ Gel DNA Recocery Kit was used. A 100 mg gel slice was dissolved in Agarose Dissolving Buffer and loaded on a Zymo-Spin Column. Centrifugation allowed collection of DNA in the column. After washing the column the DNA was eluted with nuclease-free water.

DNA Sequencing

For sequencing plasmids and PCR product samples were send to GATC Biotech. Samples were prepared according to the company's demands.

Restriction Enzyme Digestion

For most cloning strategies previous digestion of DNA is necessary. Plasmid DNA was digested with restriction endonucleases. 1 µg of DNA was digested with 10 Units of the respective enzyme. Reaction buffer was added to a total volume of 20 µl. Incubation for 1 h at 37 °C yielded satisfying results.

DNA Ligation

DNA ligation was performed using T4 ligase. 50-100 ng of the linearized backbone was mixed with1-5x the amount of the insert, 2 µl ligase buffer and 1 µl T4 ligase. Nuclease-free water was added to a total volume of 20 µl. The solution was incubated for 5-10 min at room temperature. Heating the sample to 65 °C for 10 minutes terminated the reaction. 5-10 µl were used for the transformation of bacteria.

Polymerase Chain Reaction

Polymerase chain reaction (PCR) was used to amplify a specific region of DNA defined by the primer sequence. PCR was conducted with Herculase II Fusion Enzyme with dNTP combo. 4 µl of 5X Herculase reaction buffer, 0.2 µl of dNTP mix, 0.6 µl DMSO and 0.4 µl of Herculase enhanced DNA polymerase were mixed in a PCR reaction tube. 50- 100 ng of template DNA and 1 µl of both forward and reverse primer (10 pmol/µl) were added. Nuclease-free water was added to a total volume of 20 µl. PCR was run in a thermal cycler according to the following program.

1. initiation	95.0 °C for 2:00 min	
2. denaturation	95.0 °C for 0:15 min	40x
3. primer annealing	56.0 °C for 0:15 min	
4. elongation	72.0 °C for 2:00 min	
5. final elongation	72.0 °C for 2:00 min	

In this work the primer was designed by a member of the lab in a way that it would generate a linearized plasmid with overlapping 3' termini on both ends. Linearization makes the plasmid suitable for Gibbson cloning. Additionally, the primer sequence was altered to induce a point mutation (site-directed mutagenesis).

The success of the PCR, the induction of the point mutation, was confirmed by sequencing.

Gibson Assembly

Gibson Assembly is an isothermal DNA amplification method providing for simultaneous assembly of one or multiple DNA fragments regardless of their length or compatibility. The technique was developed by Gibson et al. and works without any restriction enzyme digestion (Gibson et al., 2009). The only requirement is a 20-40 bp overlap at both ends of the DNA fragments meant to be joined. Gibson Assembly Mastermix contains three different enzyme activities. The first one is an exonuclease creating single-stranded 3´ overhangs that can anneal with overhangs of adjacent DNA fragments. The second enzyme, a DNA polymerase, closes the gaps within the annealed fragments and finally a DNA ligase covalently joins the

DNA of respective segments by sealing any possible nicks. In this work Gibson Assembly was used to seal both ends of a linearized DNA fragment undergone site-directed mutagenesis. In other words, the template was solely one fragment that needed to be circular. To conduct Gibson Assembly 1 µl of the PCR product (0.098 pmols/µl) was mixed with 10 µl of the Gibson Assembly Mastermix and 9 µl nuclease-free water. The mix was incubated at 50 °C for 15 min. E. coli were transformed with 2 µl of the reaction product and the purified plasmid was sent for sequencing.

Gateway Cloning

Gateway cloning enables the user to easily integrate different pieces of DNA incorporated in an entry vector into a certain expression system. Borrowing from integration of bacteriophage lambda DNA into *E.coli* genome the technique is based on site specific recombination (Landy, 1989). The system is composed of an entry vector containing the gene of interest and an expression vector fitted with an expression promoter and a coding sequence for ccdB. CcdB is a toxin inhibiting bacterial growth and is used for negative selection. Both the gene of interest and the *ccdB* sequence are flanked by two attachment sites called attL and attR. LR Clonase is a mixture of *E. coli*-encoded recombination proteins that recognizes these attachment sites and mediates intermolecular DNA recombination leading to a switch of the two DNA sequences flanked by the attachment sites (LR-reaction).

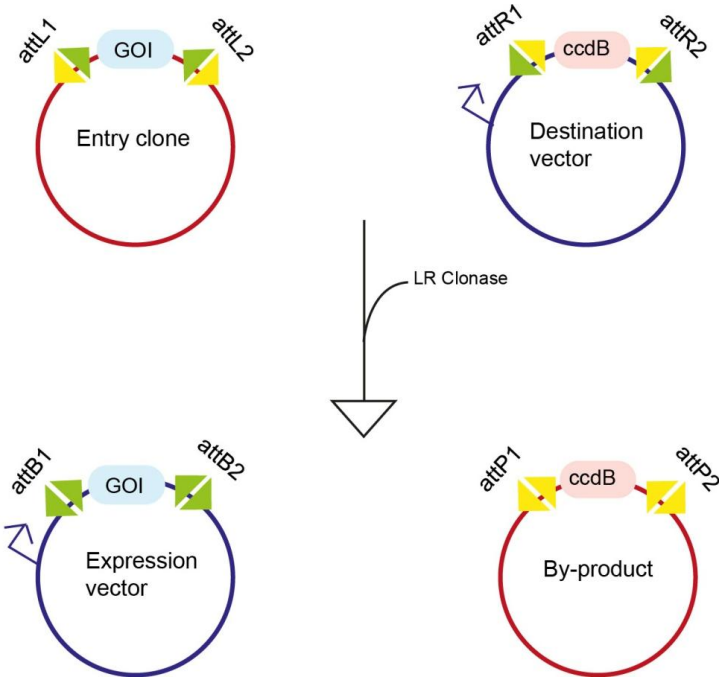

Figure 5: Gateway cloning is based on site specific recombination and enables integration of an insert of choice into a backbone vector.
Intermolecular DNA recombination is mediated by LR Clonase and occurs between the DNA sequences flanked by attachment sites. The ccdB sequence and the GOI are switched resulting in an expression vector carrying the GOI and a by-product. Figure adapted from Gateway Technology manual, Invitrogen.

LR reaction produces an expression vector carrying the gene of interest and a by-product composed of the entry clone backbone and the ccdB sequence. Transformation of bacteria with the reaction product leads to amplification of the expression vector solely since bacteria taking up the unreacted vector or the by-product carrying the ccdB sequence are prevented from growing. To facilitate the process the entry vector was linearized by restriction enzyme digestion prior to LR reaction.

For LR reaction 150 ng of the entry clone and 150 ng of the destination vector were used. 2 µl LR Clonase were added and diluted with TE buffer to a total reaction volume of 10 µl. After incubation at 25 °C for 2 h the reaction was terminated by incubation with 1 µL Proteinase K at 37 °C for 1 h. Ultimately, E. coli were transformed with 2 µl of the reaction and grown on a plate containing the appropriate selection antibiotic.

In this work, gateway cloning was carried out for two purposes. On the one hand MFN2, MFN2(R94Q) and MFN2(K109A) embedded in an entry vector were cloned into a DIO expression system and on the other hand the genetically-encoded indicators were cloned into a different expression vector.

Isolation of RNA from Eukaryotic Cell Lines

Cell samples were collected during the differentiation process and stored in 400 µl of RNA lysis buffer at -80° C. To isolate total RNA from cell lysates the ZR RNA MiniPrep^{TM} Kit was used. Work was performed in an RNase free environment. Primarily the samples were centrifuged to settle cell debris. To purify RNA the supernatant was loaded onto a column permeable for RNA and centrifuged. After centrifugation the flowthrough was diluted in ethanol and an in-tube DNase digestion was performed to eliminate any contamination with DNA. Centrifugation with a different column led to collection of the RNA in the column itself. After further washing and centrifugation steps RNA was eluted with nuclease free water and collected in an RNase-free tube.

Reverse Transcription

To translate RNA into single-stranded cDNA the High Capacity cDNA Reverse Transcription Kit was used. The Reverse Transcription Master Mix was prepared from 2 µl RT Buffer, 0.8 µl dNTP Mix, 2 µl Random Primers, 1 µl Reverse

Transcriptase and 4.2 µl nuclease-free water for each sample. 10 µl of the Master Mix were mixed with 10 µl (2 µg) of RNA and incubated in a thermal cycler for 10 min at 25 °C and 120 min at 37 °C. Heating to 85 °C for 5 minutes terminated the reaction. cDNA was stored at -20 °C for long term. For use in RT-PCR 20 µl of the reaction volume were diluted with nuclease free water to a total volume of 200 µl.

Real-Time PCR

When performing conventional PCR a DNA sequence gets amplified, indicating the presence of a certain piece of DNA. Quantification of the results can be done once the process is finished. In real time PCR on the contrary the amount of DNA is measured continuously after each cycle. This enables a much more precise analysis of the amount of PCR product and allows to conclude on the original amount of DNA. The presence of a DNA binding fluorophore increases the fluorescent signal proportionally to the amount of DNA amplified. RT-PCR was performed using forward and backward primers designed with Beacon Designer and iQ™ SYBR Green Supermix containing dNTPs, Taq Polymerase, $MgCl_2$ and SYBR® Green.

The reaction mix consisted of 4 µl template DNA (equal to 40 ng RNA template), 10 µl SYBR Green, 0.2 µl of both forward and reverse primer (200 nM) and 5.6 µl nuclease-free water. All samples were run as triplets. Expression of the housekeeping gene β-actin was measured alongside with the gene of interest in a separate set of triplets with a primer concentration of 100 nM and an annealing temperature of 59 °C. Total RNA from mouse brain served as positive control, water as negative control. DNA amplification was conducted in a thermal cycler in a defined sequence:

1. initiation	95.0 °C for 3:00 min	
2. denaturation	95.0 °C for 0:10 min	40x
3. primer annealing and elongation	58.0 °C for 0:45 min	
4. final elongation	95.0 °C for 1:00 min	
	55.0 °C for 1:00 min	

Quantitation was performed using the $\Delta\Delta C_t$- method.

3.3 Methods in Proteinbiochemistry

Immunocytochemistry

Immunocytochemistry (ICC) is a key technique to detect the presence or localization of intracellular proteins. The underlying mechanism is the capability of antibodies to specifically bind to certain antigens. Binding of a second antibody associated to a fluorophore to the first antibody leads to visualization of the structure of interest.

For ICC analysis, cells were seeded on coverslips in a 24-well plate. The next day cells were fixed in 4 % paraformaldehyde (PFA) in PBS for 20 min. After proper washing with PBS, cells were permeabilized with 0.25 % Triton X-100 in PBS for 10 min. Incubation with 10 % Rotiblock in PBS for 30 minutes prevented unspecific binding of the antibody.

The first antibody was diluted in 10 % Rotiblock in PBS enriched with 0.1 % Triton X-100 and applied to the cells at a total volume of 100 µl. Incubation at 4 °C overnight followed. After that the first antibody was discarded and the second antibody was added in the respective dilution. Cells were incubated in the dark for 1 h at room temperature. To visualize the nuclei, cells were subsequently stained with 300 nM DAPI for 3 min. To complete the process, cells were mounted on microscope slides with Fluorescent Mounting Medium. After each incubation step cells were thoroughly washed with PBS twice. Finally, the staining was evaluated using confocal microscopy. The antibodies used and the respective dilution are listed in chapter 2.1.

Immunoblot

Immunoblotting (IB) is a useful technique to visualize and quantify protein expression in a cell lysate. Initially proteins are separated by their molecular weight (SDS-PAGE). SDS is an anionic substance that linearizes protein structure and applies a negative charge to all proteins allowing separation by size regardless of charge. After separation proteins are transferred to a membrane and the protein of interest is detected with a suitable antibody. The individual steps are described in more detail below.

Acquisition of total protein lysates: Cell samples were collected during the conventional differentiation and lysed in 200 µl cold RIPA buffer substituted with protease inhibitor. 20 ml RIPA Buffer were substituted with one complete Mini Protease Inhibitor Cocktail tablet. Cell lysates were kept at -80 °C.

For quantification of the protein concentration a bicinchoninic acid assay (BCA assay) was used and the concentration was measured with a Tecan Microplate Reader. Therefore, cell debris was removed from the lysates by centrifugation for 30 min at 4 °C and maximal speed. The supernatant was used for BCA assay. To obtain equal protein concentrations the samples were diluted with an appropriate amount of nuclease-free water.

SDS-Polyacrylamid Gel Electrophoresis (SDS-PAGE): 4x LDS Sample Buffer was added to the samples. Heating to 95 °C for 5 min led to denaturation. 100 µg of the sample were loaded on a 4- 15 % Mini-PROTEAN® TGX Stain-Free™ gel next to MagicMark™ XP Western Protein Standard. Proteins were separated for 15- 17 min at 300 V.

Immunoblotting: The separated proteins on the gel were transferred to a PVDF membrane using the Trans-Blot® Turbo™ Transfer System. Staining with Ponceau S solution verified the transfer. Incubation with blocking buffer (TBS with 0.1 % Tween and 3 % powdered non-fat milk) for 1 h at room temperature provided blocking of unspecific binding sites. Proteins were visualized by immunolabelling. The primary antibody was diluted in blocking buffer and incubated with the membrane overnight at 4 °C, followed by incubation with the secondary antibodies for 1 h at room temperature the next day. After each staining and incubation step, the membrane was washed with TBS-T (TBS with 0.1 %Tween) for 10 min three times. The antibody signal was detected using the Odyssey Sa Infrared Imaging System.

Flow Cytometry

Flow cytometry is a high throughput laser-based technology for cell counting and sorting. Cells from a heterogeneous population are suspended and separated by hydrodynamic focusing. Once arranged in a single cell stream cells pass one or more laser beams causing scattering of light forwards and sideward. Depending on the size and the granularity of the cells a characteristic pattern of scattering is caused. The scattered light is conducted through several filters and mirrors until light of a

certain wavelength reaches the respective sensor. The signal is converted to a voltage pulse that is detected by the flow cytometer.

Moreover, flow cytometry can be used to evaluate the number of cells expressing a certain fluorescent protein, e.g. in terms of transfection control. Light emitted by a fluorophore travels the same way as sideward scattered light. The intensity of fluorescence correlates with the area under the voltage pulse. Ergo flow cytometry is a suitable technique to distinguish cell populations either based on their morphology or based on fluorescence.

In this work FACS was used to determine the amount of successfully transfected, hence fluorescent, cells. One day after transfection, cells were trypsinized and resuspended in 200 µl FACS buffer in a FACS tube. Propidium iodide (PI) is a red fluorescent counterstain that intercalates DNA and therefore only binds to cells with disrupted plasma membrane. Addition of 1 µl PI enables detection of dead cells. For each sample 10^4 cells were analyzed. Analysis of flow cytometric data was performed with FlowJo analysis software.

Statistics

Statistical analysis was performed with GraphPad Prism 6. Unless otherwise stated, data are presented as mean ± SEM. To compare multiple means one-way ANOVA was used.

4 Results

4.1 Differentiation and Characterization of Motoneurons Derived from Mouse ES Cells

4.1.1 Mouse ES Cells Equipped with a Neuronal Differentiation Module Can Be Differentiated to MNs

Studying mitochondrial behavior in neuronal cells required an appropriate model both easily accessible for transfection and still closely recapitulating conditions *in vivo*. To meet these demands, I used motoneurons directed from stem cells. Directed differentiation of stem cells provides an almost inexhaustible source of any type of specialized cell for *in vitro* studies. Mazzoni et al. developed a strategy for motoneuronal differentiation based on a differentiation module consisting of the NIL-transcriptional factors. Introduced in mouse ES cells, this module was sufficient to induce differentiation to postmitotic spinal motoneurons. The differentiation protocol combined expression of NIL-factors driven by a tetracycline-inducible promoter with the use of general inductive signals for neurogenesis (Mazzoni et al., 2013). I aimed to reproduce the differentiation protocol with iNIL-ES cells we had kindly received from the Mazzoni group and to confirm the neuronal identity of the differentiated cells.

For maintenance, iNIL-ES cells were cultured on a layer of mouse embryonic fibroblasts in order to prevent spontaneous differentiation (figure 6A). Withdrawal of the feeder cells and cultivation in suspension conditions permitted the formation of floating cell clusters, termed embryoid bodies (EBs) (figure 6B). These clusters contain cells from all three embryonic germ layers and are capable of differentiating into a multitude of mature somatic cell types (Itskovitz-Eldor et al., 2000). Exposition of EBs to doxycycline activated the expression of the NIL-transcriptional factors and initiated differentiation to MNs. Addition of retinoic acid and Smo, an activator of the Shh pathway, induced a basic program of neural differentiation. Return of the induced EBs to adherent culture conditions allowed further differentiation morphologically indicated by outgrowth of axons (figure 6D,E).

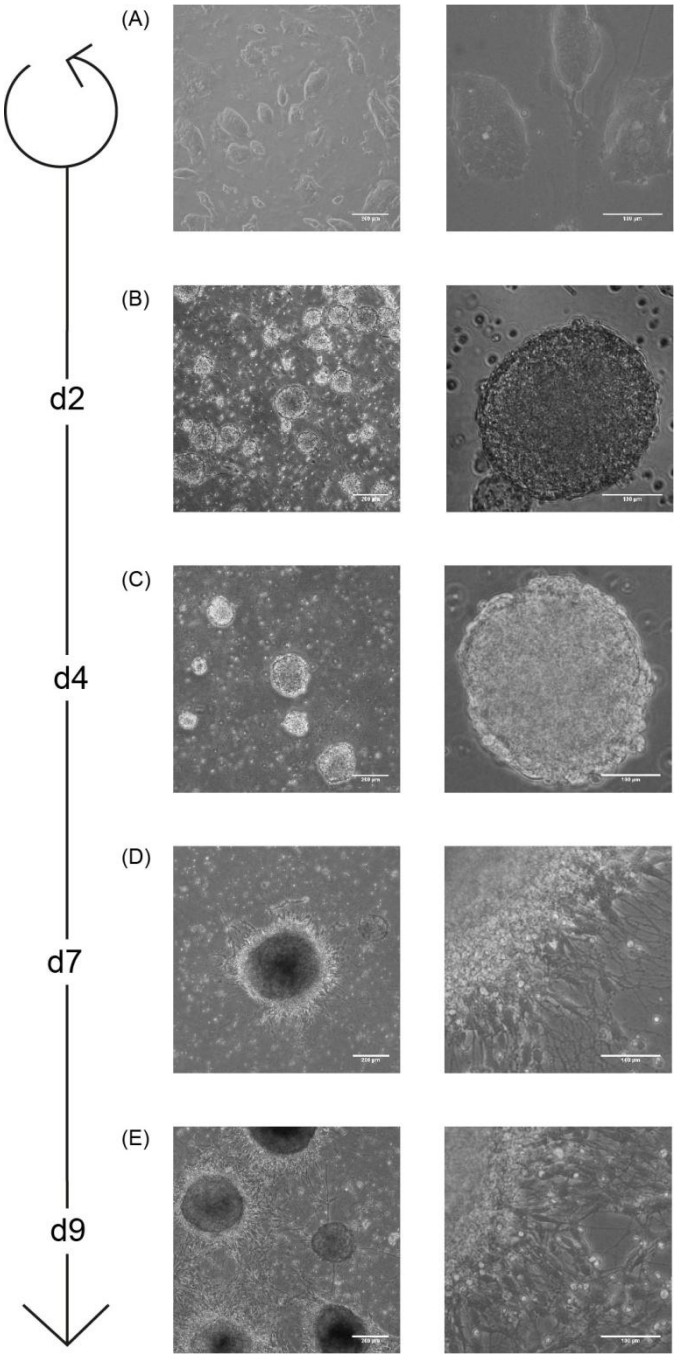

Figure 6: Culturing iNIL-ES cells in the appropriate conditions and supplementing the required factors leads to differentiation to MNs.
Brightfield images taken at the indicated points of time, scale bars represent 200 µm in the left column and 100 µm in the right column. (A) Mouse iNIL-ES cells growing in colonies on a MEF feeder layer. (B) EBs on d2 in suspension conditions. (C) EBs on d4 after stimulation with 3 µg/ml doxycyline, 1 µM RA and 0.5 µM Smo. (D) Adherent cell clusters on d7 in adhesive culture conditions. Increasing differentiation was indicated by the outgrowth of axons. (E) Further outgrowth of the axons and migration of the somata away from the cell bundle on d10. For details on the differentiation procedure see chapter 3.1.

4.1.2 ES-derived MNs Display Key Features of Mature Neuronal Cells

To assess phenotypical features of the differentiated MNs and to confirm their neuronal identity, I performed further characterization. Cell samples were taken at defined points of time during the differentiation process and analyzed for expression of the widely acknowledged neuronal marker class III β-tubulin by immunoblotting (Dráberová et al., 1998). The monoclonal TuJ1 antibody used for immunolabelling has been shown to be one of the earliest markers in neuronal differentiation and can therefore sensitively detect the increasing expression of tubulin during maturation of

MNs (Easter, JR. et al., 1993). HEK cells served as negative control. As data from two blots in figure 7B and C show, class III β-tubulin is expressed both in ES cells and in maturing MNs and expression levels seem to rise during differentiation. Data from additional differentiation processes was collected but did not show an appropriate increase in tubulin expression. Assuming that differentiation was not successful in these cells, data was excluded and statistical analysis was prevented.

Evidence for a postmitotic neuronal phenotype was given by immunostaining against Hb9 and Islet 1/2 (Isl1/2). During the embryonic period Hb9 plays a decisive role in consolidating postmitotic MN identity by governing an important developmental step in neurogenesis. The onset of Hb9 expression is coincident with Islet1 expression and MNs dropping out of the cell cycle (Arber et al., 1999). The LIM homeobox protein Isl1 is one of the first markers of neuronal differentiations and is commonly expressed by all classes of MNs (Pfaff et al., 1996). The antibody used in this work detected both Isl1 and Isl2. Counterstaining of the actin cytoskeleton with Phalloidin outlined the cellular structure. As depicted in figure 7A, expression of Hb9 and Islet1/2 in differentiated MNs on d6 was confirmed. Islet 1/2 expression was restricted to the nucleus mainly, consistent with its role as a transcriptional factor. Hb9 expression however, as depicted in figure 7A, was primarily detected in the cytoplasm. While there are reports indicating a both nuclear and cytoplasmatic distribution of Hb9 at certain stages during motoneuron differentiation (Leotta et al., 2014), the complete lack of Hb9 within the nucleus in this work might partly reduce the reliability of the characterization. Together, these data still point to a postmitotic motoneuronal identity of the differentiated cells.

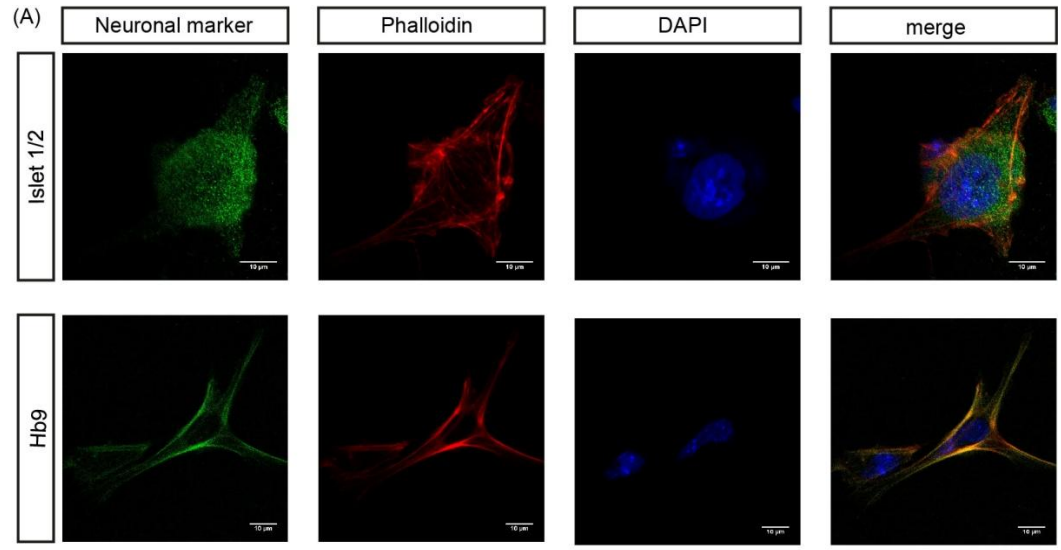

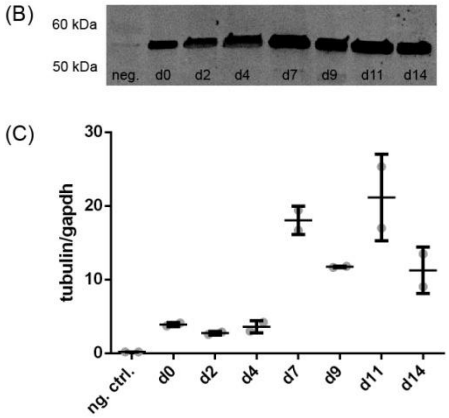

Figure 7: ES-derived MNs express motoneuronal proteins. (A) Immunostaining of ES-derived MNs on d6 against Hb9 and Islet 1/2 confirmed neuronal identity of the differentiated cells. Counterstaining with Phalloidin visualized the actin cytoskeleton. Scale bars represent 10 µm. (B) Expression of the neuronal marker class III β-tubulin in differentiating MNs was confirmed by immunoblotting. Cell samples were taken on the indicated points of time and stained with anti-neuron-specific-β-III tubulin. HEK cells served as negative control (ng. ctrl.). Gapdh served as loading control. (C) Quantification of two immunoblots. Data are presented as mean ± SEM. Quantification was performed from two independent blots.

4.1.3 Neuronal Identity Can Be Confirmed in NPC- derived MNs

Successful differentiation of mESCs to mature MNs provided us with a tool to study the Charcot-Marie-Tooth-related protein MFN2 and the influence of mutated MFN2. In order to meet this objective, I aimed to find a suitable transfection strategy. In a first approach, cells were transfected at the end of the differentiation protocol. Growing in clusters and being postmitotic at this stage of differentiation, uptake of the plasmid by differentiated MNs was not successful (data not shown). Transfection of ES cells before differentiation on the other hand, failed since the cells lost almost all of the plasmid due to cell division during the differentiation process. In the conventional Mazzoni differentiation protocol, differentiating cells bypass any progenitor stage. We therefore introduced an intermediate step to the protocol, that served to generate a state were cells were still dividing and simultaneously shortened the time period between transfection and differentiation endpoint. INIL-mESC cells

were differentiated to neuronal progenitor cells (NPCs) by a member of the lab, Dr. Alireza Pouya, according to a previously established protocol (Fazeli et al., 2013).

NPCs can be easily propagated in cell culture and pose a readily available source for the generation of mature neuronal cells. Propagation of NPCs *in vitro* is strictly dependent on the presence of basic fibroblast growth factor (bFGF). Withdrawal of the mitogen, as when NPC medium is switched to MN medium, induces further neuronal differentiation (Okabe et al., 1996). Additionally, doxycycline was administered for the first three days to switch on the iNIL-differentiation module. For detailed information on the differentiation protocol see chapter 3.1. To demonstrate that NPC-derived MNs were equally qualified for further studies cells were evaluated immunohistochemically for neuronal surface markers. NPC- derived MNs on day 10 were immunoreactive for the neuronal markers Tubulin, Hb9 and Islet1/2 (figure 8B) which confirmed their neuronal identity.

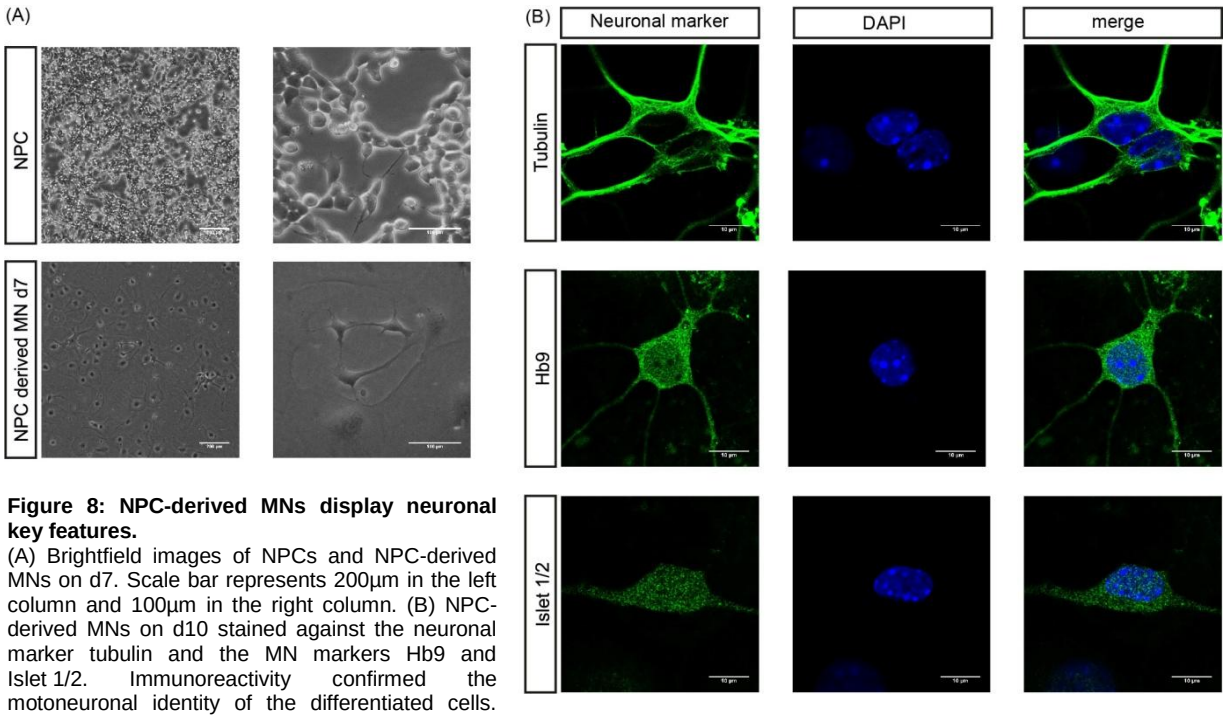

Figure 8: NPC-derived MNs display neuronal key features.
(A) Brightfield images of NPCs and NPC-derived MNs on d7. Scale bar represents 200µm in the left column and 100µm in the right column. (B) NPC-derived MNs on d10 stained against the neuronal marker tubulin and the MN markers Hb9 and Islet 1/2. Immunoreactivity confirmed the motoneuronal identity of the differentiated cells. Scale bars represent 10µm.

4.1.4 Endogenous MFN2 Expression Is Detectable During the Entire Differentiation Process

To further confirm that both ES-derived and NPC-derived MNs are suitable models to study MFN2, I evaluated endogenous MFN2 mRNA expression by RT-PCR in these cells. The experiment was performed with cell samples collected both during the conventional differentiation program and the modified protocol with an NPC interim stage. RNA was extracted and transcribed to cDNA. For quantitative analysis of the RT-PCR data, ΔCt values of the target gene were normalized to ΔCt values of the internal loading control, β-actin. The expression level of each sample was then compared to baseline MFN2 expression in ES cells. The transcript was detectable at all points during differentiation confirming that differentiated MNs are a reliable model to study the role of MFN2 on mitochondrial bioenergetics.

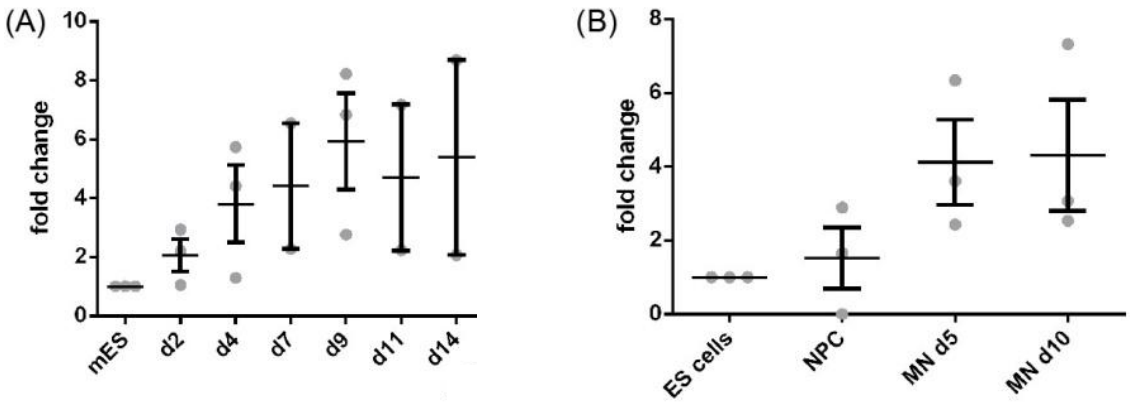

Figure 9: RT-PCR analysis confirms MFN2 gene expression during the whole differentiation process.
(A) Expression level of MFN2 during the conventional differentiation process. MFN2 expression was detectable throughout the whole differentiation process. (B) MFN2 expression during differentiation from NPCs to MNs. MFN2 expression was detectable both on NPC stage and on MN stage. Data were obtained from three independent experiments. Each sample was run as triplet. Total RNA was extracted from cell samples collected during the differentiation process. Total mouse brain mRNA served as positive control (pos. ctrl). Data are presented as mean ± SEM. Relative quantitation was performed using the $\Delta\Delta C_t$ method. MFN2 expression was adjusted to the endogenous control target, β-actin. Means were compared using one-way ANOVA. At a significance level of $p<0.05$ the results were not statistically significant.

4.2 Lipofectamine 2000 is the Most Suitable Reagent for the Transfection of NPCs

To produce reliable results in further experiments it was pivotal to achieve sufficient transfection efficiency. In order to optimize transfection conditions, three different reagents in different ratios of DNA and reagent were compared: Lipofectamine 2000, Lipofectamine 3000 and Effectene. All three reagents are based on the formation of DNA-lipid-complexes.

NPCs were seeded in a 12-well plate and transfected with a test plasmid coding for the yellow fluorescent protein Venus with one of the three reagents. The following day the number of transfected cells was assessed by flow cytometry. Untransfected NPCs served as negative control. As demonstrated in figure 10, the best transfection performance was achieved with Lipofectamine 2000 in a DNA/reagent ratio of 1/2.5. Further transfections were performed using this setup.

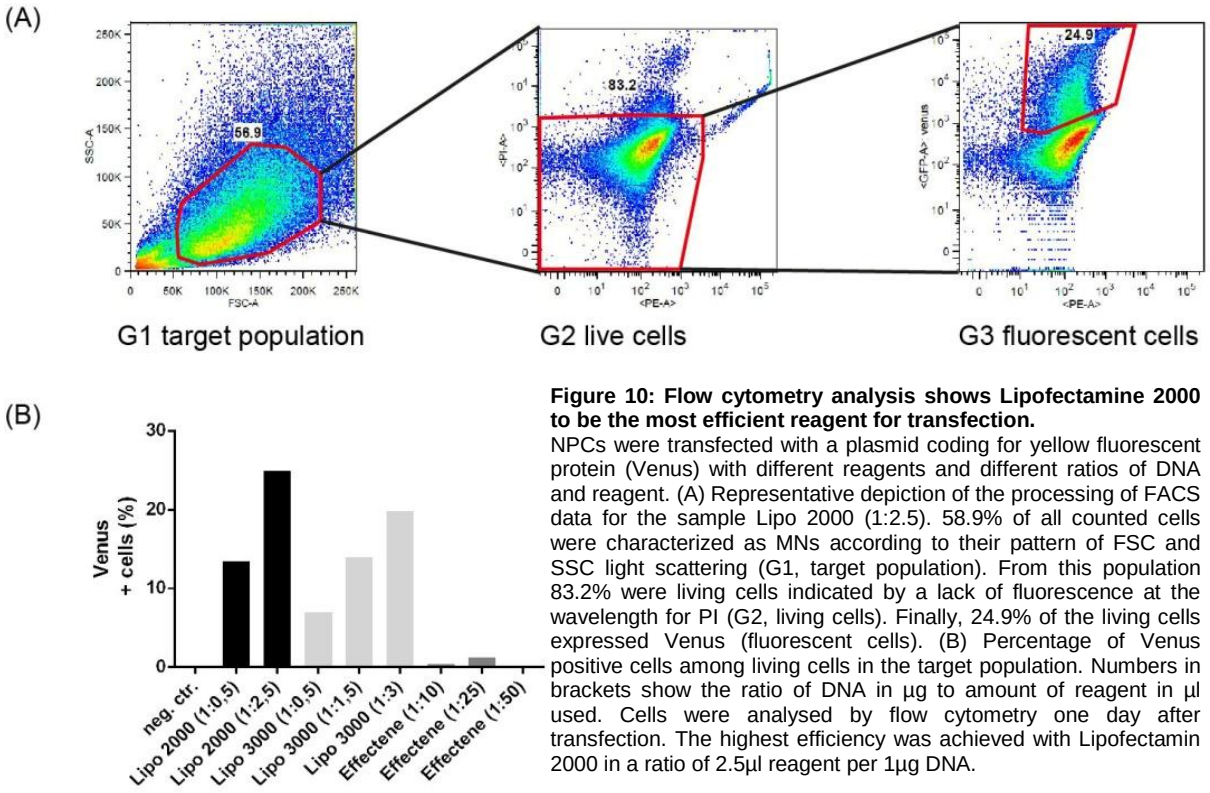

Figure 10: Flow cytometry analysis shows Lipofectamine 2000 to be the most efficient reagent for transfection.
NPCs were transfected with a plasmid coding for yellow fluorescent protein (Venus) with different reagents and different ratios of DNA and reagent. (A) Representative depiction of the processing of FACS data for the sample Lipo 2000 (1:2.5). 58.9% of all counted cells were characterized as MNs according to their pattern of FSC and SSC light scattering (G1, target population). From this population 83.2% were living cells indicated by a lack of fluorescence at the wavelength for PI (G2, living cells). Finally, 24.9% of the living cells expressed Venus (fluorescent cells). (B) Percentage of Venus positive cells among living cells in the target population. Numbers in brackets show the ratio of DNA in µg to amount of reagent in µl used. Cells were analysed by flow cytometry one day after transfection. The highest efficiency was achieved with Lipofectamin 2000 in a ratio of 2.5µl reagent per 1µg DNA.

4.3 Cell-Type Specific Overexpression of MFN2 in Differentiated MNs Can Be Achieved Using a DIO Gene Expression System

After confirming that differentiated spinal MNs were an appropriate tool to study MFN2 and identifying the most suitable reagent for overexpression, my next goal was to find an experimental setup strictly limiting expression to motoneuronal cells. The cell population arising from directed differentiation of ES cells, however, did not purely consist of spinal MNs. To avoid any bias, I chose a double-floxed inverted orientation (DIO) gene expression system for the overexpression of MFN2.

DIO gene expression is a convenient technique for selective overexpression based on Cre-loxP recombination (Sohal et al., 2009). Cre-loxP recombination takes advantage of the fact that site specific recombination can occur between homotypic but not heterotypic lox-sites (Branda and Dymecki, 2004). The target gene, MFN2, is

placed on a plasmid in antisense orientation and flanked by two incompatible pairs of Lox-sites facing each other, loxP and lox2722 (figure 11A). In this state transcription is prevented. If Cre recombinase is translated from a second plasmid and expressed simultaneously, the protein recognizes the lox sites and mediates irreversible inversion of the target gene in a two-step procedure. In a first step, inversion occurs between loxP sites, placing the expression cassette in sense orientation but still prone to further inversion. The first reversible step then enables an excision step leading to a permanent inverted state (figure 11B). As a result, the expression cassette is placed in sense orientation flanked by two incompatible lox sites ergo ready for transcription and protected from further inversion (figure 11C).

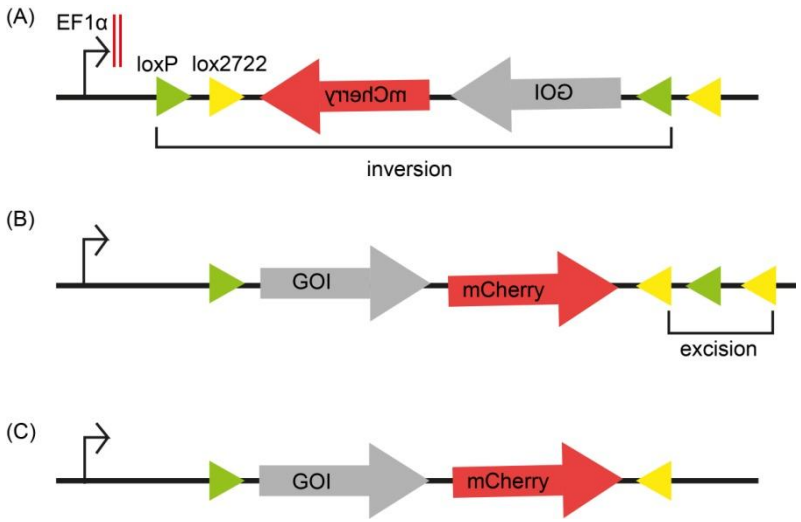

Figure 11: DIO gene expression is conducted as a two-step process based on site specific recombination.
(A) The expression cassette composed of the target gene (gene of interest, GOI) and mCherry is placed between two pairs of heterotypic lox sites (loxP and lox2722). Antisense orientation prevents transcription. Recombination is then mediated by Cre recombinase in a bipartite process. First, inversion occurs between loxP sites leading to a change of orientation of the expression cassette and the inner lox sites. (B) This puts the lox2722 sites in the same orientation and enables a second excision step. (C) The expression cassette is now in sense orientation and flanked by two heterotypic lox sites. Transcription is possible and further inversion is prevented.

To restrict expression of MFN2 to motoneuronal cells, Cre recombinase was under control of the MN-specific Hb9 promoter (Arber et al., 1999). In this way, only MNs were capable of expressing Cre recombinase and conducting the recombination process (figure 12A). To identify successfully transfected cells and to distinguish them from MNs endogenously expressing MFN2, nuclear mCherry, a red fluorescent protein, was expressed along with MFN2 on the DIO vector.

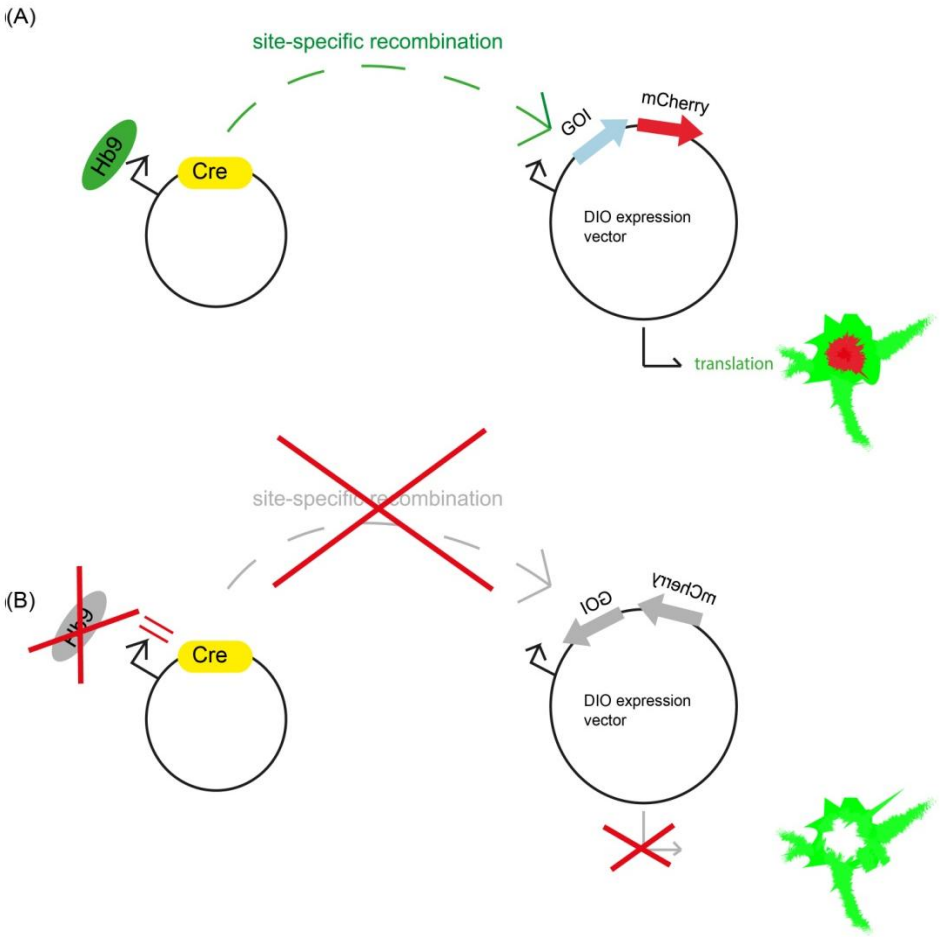

Figure 12: Cell-type specific overexpression through a DIO expression system relies on the presence of motoneuronal Hb9.
(A) Expression of Hb9 is a prerequisite for the translation of Cre recombinase. Expression of Cre, in turn, promotes a two-step inversion process resulting in transcription of the target gene (gene of interest, GOI). The gene of interest, MFN2, is accompanied by a coding sequence for nuclear mCherry. Successful expression of the GOI can be visualized by a nuclear mCherry signal. (B) In non-motoneuronal cells lacking Hb9, expression of the target gene is prevented. Failed overexpression is indicated by a lack of nuclear mCherry.

Specifically, NPCs were transfected with the DIO expression vector coding for MFN2 and a second Hb9-driven plasmid coding for Cre. Differentiation was induced the following day as described in chapter 3.1. On d5 and d10 differentiated MNs were fixed in PFA and immunostained. Staining against mCherry was conducted to assess successful overexpression and circumvent the possibility of detecting low levels of endogenous MFN2. Protein expression was then evaluated by fluorescence microscopy. As shown in figure 13, immunostaining confirmed the presence of nuclear mCherry in differentiated MNs. MFN2 itself was ubiquitously expressed, consistent with previous findings that MFN2 is a mitochondrial protein, hence located in the cytoplasm (Santel and Fuller, 2001). Mouse hippocampal HT22 cells transfected with the same DIO vector coding for MFN2 and a second vector coding for Cre recombinase driven by a ubiquitous CAG promoter served as positive control.

Compared to HT22 cells, the fluorescent mCherry signal was considerably lower in MNs on d5 and barely detectable on d10. Additionally, the staining intensity for MFN2 in differentiated MNs was also lower than in the control cells. These data confirmed that selective overexpression of MFN2 in spinal MNs can be achieved using a DIO gene expression system but at the cost of gradual decline in expression levels over time, indicated by a fainting signal. Therefore, analysis of transfected NPC-derived MNs was conducted on d5 rather than on d10.

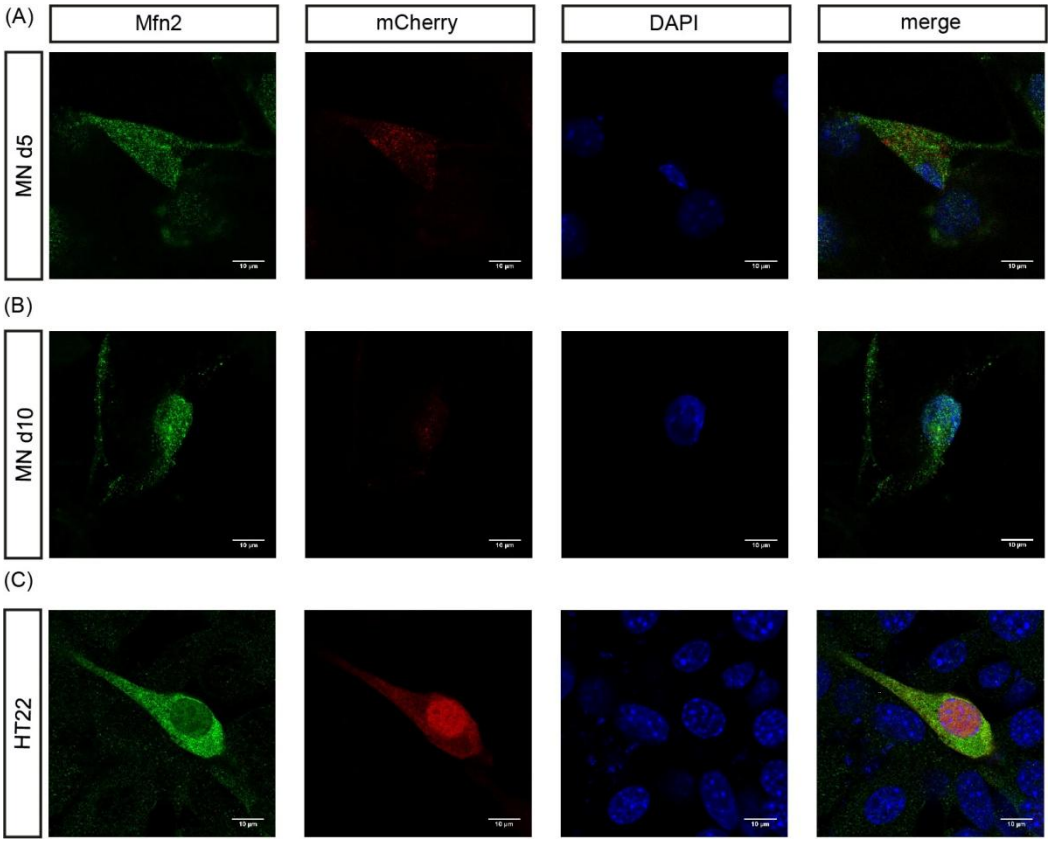

Figure 13: Protein expression after transient transfection of NPCs outlasts the differentiation process.
(A, B) NPCs were transiently transfected with a DIO-expression vector coding for MFN2 and a second plasmid coding for Cre recombinase driven by a Hb9 promoter. Differentiation was induced one day after transfection. On d5 and d10 a subset of cells was fixed and stained against MFN2 and red fluorescent protein. Visualization of the staining was performed by confocal microscopy. (C) HT22 cells served as control. Scale bars represent 10 µm.

4.4 Intracellular Metabolism in MFN2 Expressing MNs Can Be Monitored Using Genetic Indicators

Pich et al. provided evidence that MFN2 can influence cellular metabolism (2005). In particular, they could show that MFN2 overexpression leads to increased expression of several components of the OXPHOS system and increased glucose oxidation in general. Based on these findings, I aimed to evaluate metabolic behavior in MNs carrying mutations in MFN2 and to compare them to MNs overexpressing the wild

type protein. I considered both the disease-causing mutation R94Q and the GTPase mutant version K109A. Specifically, I examined the ATP and the lactate concentration in the mentioned cell populations.

Monitoring of metabolic processes was performed using genetically-encoded indicators. Genetically-encoded indicators render great services in visualizing and quantifying intracellular events in living cells. Leading principles in this technology are circular permutation of a fluorescent protein or fluorescence resonance energy transfer (FRET) technology (Germond et al., 2016). The indicators used in this work were FRET based. FRET technology is composed of two fluorophores of overlapping absorption spectra connected through a sensing domain for the respective biological substrate. Depending on the distance of the two fluorescent proteins, a certain amount of energy is transferred from one (donor) to the other (acceptor) fluorophore (Förster, 1948). If the concentration of the respective ligand in the solute environment changes, the sensing domain promotes a spatial approach of the donor and the acceptor, which then leads to a change in FRET efficiency and subsequently to a change in the fluorescence spectrum. A graphical representation of the process can be found in figure 15E. In this work, two different genetically-encoded indicators were used. *Laconic* is an indicator for quantification of the intracellular lactate concentration. The sensor is composed of a teal fluorescent protein (mTFP) and a yellow fluorescent protein (Venus) linked by a sensing domain, derived from LldR, a bacterial transcription regulator (San Martin et al., 2013). The second sensor used was *AT1.03*^{YEMK}, a real time ATP-monitor. The sensing domain is based on the ε-subunit of the bacterial F_0F_1-ATP synthase and connects a cyan fluorescent protein (mseCFP) with a yellow fluorescent protein (mVenus) (Imamura et al., 2009). Both indicators were cloned into piggyBac expression vectors driven by a CAG promoter using gateway cloning.

Wild type or mutated MFN2 was overexpressed using a DIO expression system as described in the previous chapter. Therefore, NPCs were transfected with the three plasmids, listed below.

pAAV-mHb9-miniCMV::Cre	Cre recombinase driven by a Hb9 promoter
pAAV-EF1α::DIO-HA-gene of interest-DEST-IRES-mcherry-NLS	DIO expression vector fitted with the gene of interest (MFN2-wt, MFN2-R94Q, MFN2-K109A) and nuclear mCherry under the control of an EF1α promoter
pPB-CAG::HA- indicator	PiggyBac expression vector fitted with the respective indicator (AT1.03YEMK or Laconic)

For a better understanding, figure 14 shows a schematic representation of the experimental setup.

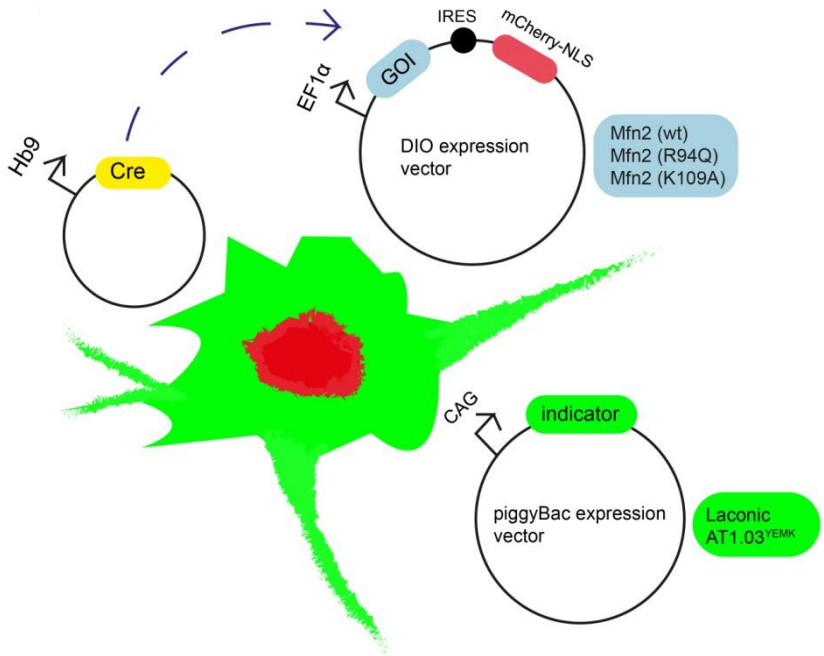

Figure 14: Multiple plasmids are necessary to analyze metabolic behavior in target cells.
The vector system is composed of three plasmids. The first two plasmids, a DIO expression vector and the vector coding for Cre, govern selective overexpression of the GOI (MFN2(wt), MFN2(R94Q) or MFN2(K109A), as described in chapter 4.3. The third plasmid, a piggyBac vector, harbors a genetically encoded indicator and is capable of monitoring intracellular metabolic processes. MNs that have successfully been transfected with all parts of the vector system can be identified by a nuclear mCherry signal and fluorescence in the respective channels for each indicator. NLS= nuclear localization sequence, IRES= internal ribosome entry site.

Transfection of NPCs with the three plasmids was conducted in a 6-well plate with Lipofectamine 2000. The following day the transfected cells were replated on ibidi slides and differentiation was induced as described. On d5 live cell imaging was performed to measure the fluorescence signal. Cells were imaged at room

temperature using a TCS SP5 confocal microscope (figure 15A). Only cells both showing fluorescence in the respective channels for the indicator and exhibiting a red nucleus were included. Fluorescence intensity was measured using ImageJ and the respective ratio was calculated. Compared to the empty vector controls, neither MNs overexpressing wt MFN2 nor cells overexpressing the mutated protein showed a significant difference in lactate and ATP levels (figure 15B,C).

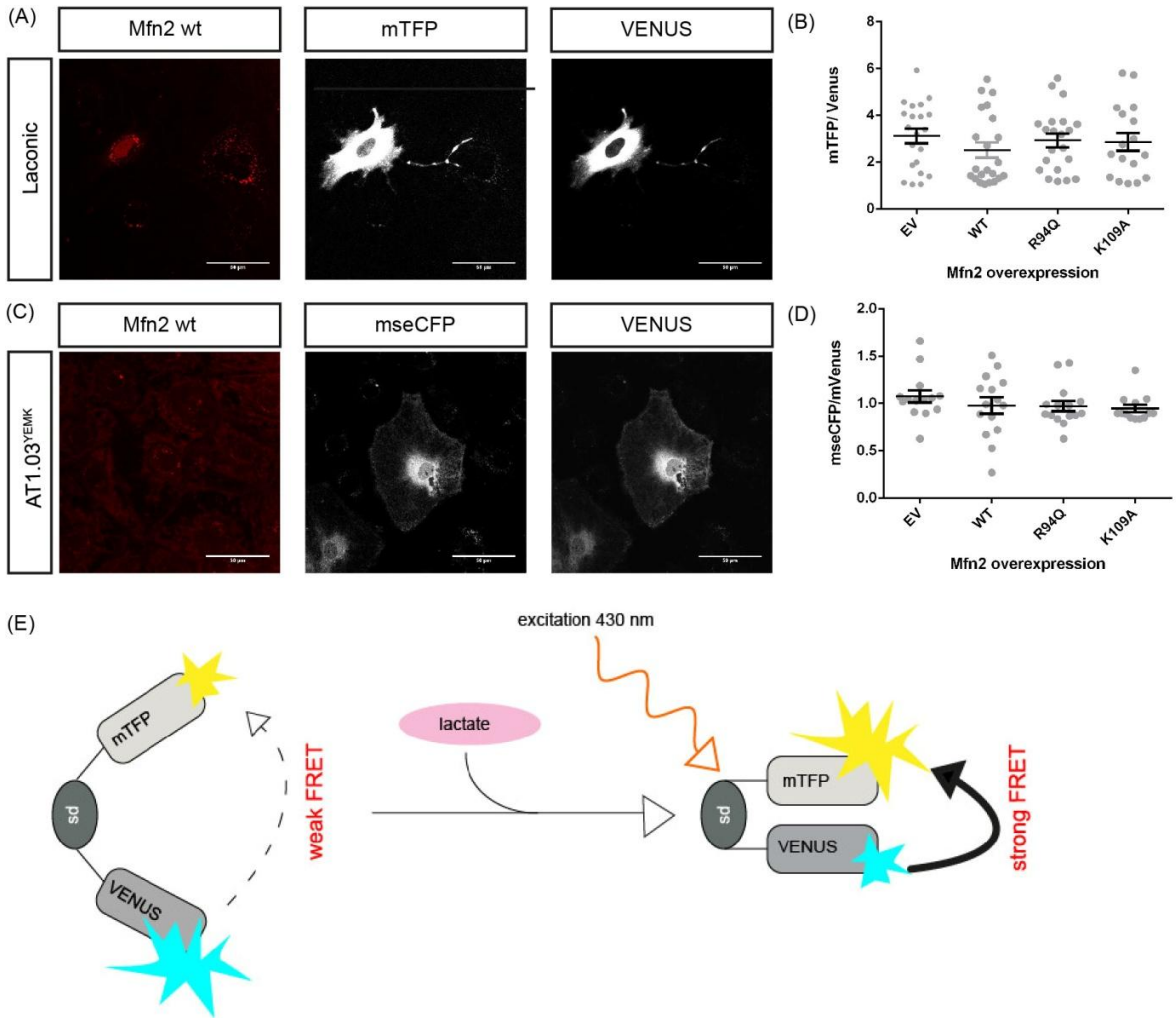

Figure 15: Transient overexpression of wt or mutated MFN2 has no significant impact on lactate and ATP level.
Cells were transfected with wt or mutated MFN2 and the respective indicator as NPCs and differentiated to MNs. (A), (C) Exemplary representation of confocal images taken on d5. Transient overexpression of MFN2 in adult MNs is recognizable by expression of nuclear mCherry. Cells expressing Laconic (A) were excited at 430nm and emission of mTFP and Venus was measured at 485 and 528 nm. Cells expressing AT1.03 ^{YEMK} (C) were excited at 435nm, emission of Venus and mCFP was recorded at 527 and 475 nm. (B), (D) For each group, approximately 20 cells were analyzed by measuring fluorescence intensity with ImageJ. Data are presented as mean ± SEM. Means were compared using one-way ANOVA and Dunnett's multiple comparisons test. Compared to the empty vector (EV) no significant difference in lactate or ATP concentration is detectable for both indicators, neither in cells expressing WT nor mutated MFN2. (E) Schematic representation of the operating principle of the FRET based indicator Laconic. An increase in the lactate concentration of the solute environment leads to an approach of the donor and the acceptor fluorophore. Excitation of the cells at 430nm shows the subsequent change in the fluorescence intensity.

5 Discussion

The main objective of this work was to generate motoneurons from mouse embryonic stem cells and to implement a suitable strategy for overexpression of the mitochondrial protein MFN2 in these neurons. The second objective was to introduce genetic indicators into these cells in order to evaluate potential metabolic changes associated with the CMT2A-related mutation $MFN2^{R94Q}$. Establishing a transfection strategy which ensured reliable expression of both proteins involved several complexities that will be discussed below.

5.1 Introduction of a NPC Interim Stage in Directed Differentiation of ES Cells Facilitates Transfection

Previous reports showed that *in vitro,* mES cells can be differentiated to spinal MNs by overexpressing the NIL transcriptional factors and providing the respective patterning signals (Wichterle et al., 2002; Mazzoni et al., 2013). Since CMT selectively affects spinal motor neurons I assumed that these differentiated cells were suitable for investigating the effects of CMT-associated MFN2 mutations (Cartoni and Martinou, 2009). I confirmed that ES-derived MNs display phenotypical properties of mature neuronal cells (Mazzoni et al., 2013). Furthermore, I showed that MFN2 is endogenously expressed during the whole differentiation process. This allowed to conclude that differentiated motoneurons were a reliable model for further studies on MFN2.

To establish a suitable strategy for the overexpression of MFN2, multiple variables during transfection can be modified. In this work mainly two parts were taken into consideration: The point of time during the differentiation process and the method of transfection. With regard to the first, it is important to know that compared to solely RA- and Shh-generated MNs, induced MNs bypass any progenitor stage in their differentiation process (Mazzoni et al., 2013). Consequently, to establish overexpression of MFN2, cells can be transfected either in the beginning as dividing ES cells or at the end of the differentiation process as postmitotic MNs. Transfecting mature motoneurons had two drawbacks. On the one hand, at an advanced stage of differentiation cells grew in clusters which spatially compromised the accessibility for the DNA-liposome complex to cells. On the other hand, differentiated neurons were postmitotic. Normally, DNA enters the nucleus during mitosis once the nuclear membrane breaks down. Postmitotic, non-dividing cells are therefore harder to

transfect, yielding single-digit percentage in transfection efficiency (Karra and Dahm, 2010). Indeed, transfection of differentiated postmitotic MNs was not successful (data not shown). Since the differentiation protocol required several days, I assumed that transfecting cells on ES stage posed a problem as well, since cells would lose most of the plasmid during the course of differentiation. To avoid both concerns, we introduced an intermediate step in the differentiation protocol. A colleague of mine, Dr. Alireza Pouya, differentiated ES cells to neural progenitor cells (NPCs). Neuronal progenitor cells grow separately and are still dividing and therefore more susceptible to transfection (Okabe et al., 1996). Previous data showed that NPCs can be transfected with an efficiency up to 60-80 % without showing abnormalities in subsequent differentiation to neuronal cells (Dieterlen et al., 2009). Additionally, transfection of NPCs instead of ES cells had the advantage to shorten the interval between transfection and end of differentiation and thereby prevent loss of the plasmid. I confirmed that MNs differentiated from NPCs expressed the same neuronal markers as MNs differentiated from ES cells and were therefore equally suitable for further studies.

5.2 Transfection of NPCs Is Possible with Lipofectamine 2000 at the Cost of Low Efficiency

After determining the appropriate point of time for transfection the next step was to find a suitable reagent. For transfection of nucleic acid into mammalian cells, a whole range of options is available. Mainly, the methods can be divided into viral and non-viral approaches. The choice of the appropriate method depends on the purpose of transfection. In this work, introducing three plamids into the target cells and measuring metabolic changes in these cells required both high transfection efficiency and very low disturbance of the physiological conditions. To meet both conditions, two different non-viral methods were taken into closer consideration: Nucleofection and lipofection.

Nucleofection is a developed version of electroporation. During nucleofection, nucleic acid directly enters the nucleus of a cell with the help of a high voltage pulse (Karra and Dahm, 2010). This method promises high transfection rates in human NPCs of up to 60-80 % (Dieterlen et al., 2009). The main drawback however, is the high technical effort and potential disturbance of cell physiology, which makes it more suitable for applications were quantity is more important than maintaining

physiological conditions (Karra and Dahm, 2010). Lipofection, on the other hand, is a commonly used and simple technique. Transfection efficiency of 20-30% has been reported in primary neurons (Dalby et al., 2004). This method tolerates the presence of serum during the transfection process and has only minor cytotoxic effects. Consequently, I assumed that this was the most suitable method to assess metabolic function after transfection. I therefore compared different reagents based on lipofection and in a second step, different concentrations of DNA and transfection reagent regarding their transfection efficiency in NPCs. The highest expression level of the test plasmid was achieved with Lipofectamine 2000 in a DNA/reagent ratio of 1/2.5, as evaluated by flow cytometry. With this setup, 24.9 % of living neuronal cells expressed the respective fluorescent protein which is similar to values previously described. In relation to potential therapeutic consequences lipofection offers a further advantage. It can be assumed that, compared to viral transduction, gene delivery by lipofection reduces the risk to induce mutations and initiate an immune response (Karra and Dahm, 2010).

However, considering that in the final experimental setup the target cell needs to take up three plamids simultaneously, virus-based methods might be needed to further increase transfection efficiency. Because of their neurotropism, adeno-associated viruses (AAVs) are most commonly used for both *in vivo* and *in vitro* gene delivery in neurons (Bartlett et al., 1998). In a long term perspective, AAVs are comparatively suitable for clinical applications in the field of gene therapy because of their low tendency to induce immune responses and their nonpathogenicity (Büning et al., 2008). Transduction of primary cultured hippocampal neurons with AAV *in vitro* was conducted with an efficiency of 94% (Royo et al., 2008). Apart from their high efficiency, AAVs have another advantage. Using lipid-based methods for transfection, I observed a strong decrease in MFN2 overexpression over the course of time. In contrast, transduction with AAVs leads to stable genomic integration and induces high transduction levels for up to 8 weeks (Royo et al., 2008). Nevertheless, there are drawbacks to viral transduction. The small genome size of the virus-based vectors limits insert size to maximal 5kb (Washbourne and McAllister, 2002). Furthermore, viral transduction is inferior to lipofection regarding the strategy for generating vectors. In this work, gateway cloning was used to incorporate inserts into the expression vector, which allowed us to quickly and easily generate different versions of one vector. This gave us the opportunity to produce a vast amount of

different genetic indicators from the same backbone and in turn gave us a powerful tool to explore almost any metabolic alteration possibly associated with CMT. Using this technique does not only enable us to quickly change the genetic indicator but also the overexpressed mitochondrial protein. We can thereby repeat the experiments with other mutated proteins associated with CMT like Ganglioside-induced differentiation-associated protein-1 (Gdap1) (Baxter et al., 2002). Using viral technique on the other hand nullifies this advantage since it would be necessary to produce a distinct virus for each indicator or mitochondrial protein in a time consuming and demanding manner.

5.3 Genetic Indicators Cannot Detect Significant Metabolic Differences in MNs Expressing Wild Type or Mutant MFN2

In order to unravel the effect of CMT2A on cellular metabolism, I introduced genetic indicators into neuronal cells and compared three groups of neurons: Neurons overexpressing wild type MFN2, neurons expressing mutated MFN2 and neurons expressing an empty vector. In each of these groups, lactate concentration and ATP level were assessed.

We know that MFN2 plays a decisive role in energy metabolism. Repression results in diminished glucose oxidation, reduced cellular respiration and increased lactate production (Bach et al., 2003; Pich et al., 2005). Loiseau et al. revealed a mitochondrial coupling defect and decreased membrane potential as a cause for reduced OXPHOS efficacy in CMT2A patients carrying mutations in MFN2 (Loiseau et al., 2007). Interestingly, ATP production is preserved in MFN2-deficient cells by an increase of the basal rate of cellular respiration (Pich et al., 2005). Overexpression of MFN2, induces subunits of the OXPHOS system and increases fuel oxidation and membrane potential (Pich et al., 2005). Concluding from these results I expected to detect a difference in cellular energy metabolism upon overexpression of wild type MFN2 and aimed to assess further changes in cells expressing mutated MFN2. However no difference was detected in both ATP level and lactate concentration in each of the three groups. The fact that the ATP level was unaltered is concordant with previous findings that MFN2 overexpression has an influence on cellular respiration but affected cells manage to sustain ATP levels by increasing basal respiration (Pich et al., 2005). However, the lack of difference in lactate concentration was unexpected.

To collect additional evidence on this question lactate could be measured with a different method. Conventional methods for lactate measurement largely rely on enzymatic reactions and subsequent photometric detection (San Martin et al., 2013). For this purpose various commercial assay systems are available. However, these assay system require destruction of the sample to measure intracellular lactate. Operating on a genomic level and being able to measure intracellular lactate in intact live cells, genetic indicators are more suitable to measure metabolic changes. Considering that the lactate sensor Laconic has been shown to detect lactate levels in a wide range of 1 µM to 10 mM and thereby covering the physiological range of lactate concentration it appears unlikely that the reporter is not sensitive enough to detect an existing difference in the single cell (San Martin et al., 2013). Still, enzymatic methods might be an option to corroborate information provided with the use of genetic indicators.

In this work quantification of the fluorescence signal emitted by the genetic indicator was performed by manually imaging single cells with confocal microscopy and analyzing fluorescence intensity with an appropriate program. Since live cell imaging is very time-consuming the number of cells that can be imaged at a time is limited. Considering that I included approximately 20 cells for each group, we cannot rule out the possibility that the number is too low to detect a significant difference. One possibility to overcome this problem is the use of high-throughput screening systems. High-throughput fluorescence microscopy enables us to automatically measure fluorescence intensity in intact living cells in large numbers and to simultaneously evaluate the intensity with less biased automatic processing methods (Pepperkok and Ellenberg, 2006). To identify the appropriate cells, high-throughput imaging systems require a robust level of gene expression both qualitatively and quantitatively. However in this work, largely due to the fact that the cell needs to take up three plasmids at a time, these demands regarding transfection efficiency were not met. Once we find a way to improve transfection efficiency, high-throughput microscopy will enable us to quickly generate data on a much larger scale than manually possible thereby creating new opportunities in efficiently monitoring metabolic changes with different genetic indicators.

5.4 Differentiation to MNs in the Context of a Larger Picture: What Can Directed Differentiation Offer in the Understanding of Neurodegenerative Diseases?

To fully understand how mutations in mitochondrial proteins cause neurodegeneration further studies are necessary. Neuronal tissue of affected patients might be the most reliable tool for these studies. However, in the human body neural cells cannot easily be accessed and biopsies of the neural tracts of affected individuals involve high risks for the patient. Utilizing human fetal tissue from spare embryos from *in vitro* fertilization as sources of cells for the differentiation of MNs is hindered by ethical concerns and legal limitations. To circumvent both problems, research made use of a very elegant and much gentler method for the generation of patient-derived neuronal cells. Takahashi et al. established a protocol for the generations of pluripotent stem cells from human dermal fibroblasts, termed induced pluripotent stem cells (iPS cells). Transduction with four defined factors reprogrammed cells to an undifferentiated state (2007). On that basis, Hester et al. implemented an approach to generate functional MNs from human iPS cells through overexpression of the NIL transcription factors and substitution with the respective patterning signals (Hester et al., 2011). Disease-specific motoneurons from patient derived fibroblasts display CMT-associated changes in cellular metabolism most precisely and are therefore the most suitable model to study the role of MFN2 mutations in the pathogenesis of CMT. Measuring metabolic changes in patient-derived motoneurons might lead to more reliable results compared to directed motoneurons from ES cells. Since these cells express mutated MFN2 endogenously, artificial overexpression becomes redundant. As a consequence only the genetic indicator needs to be introduced instead of three plasmids, thus hopefully improving transfection efficiency. To make sure that the metabolic changes in these cells are in fact attributable to a mutation in MFN2 it will be necessary to repeat the experiment in MFN2 KO cells.

Finally, differentiation to specific cell types like MNs from iPS cells provides an almost infinite pool of cells for drug screening and development of stem cell-based therapeutic strategies in a field with very limited treatment options. In the last decades stem-cell based approaches for the therapy of motoneuron diseases have achieved a great deal. In a mouse model for spinal muscular atrophy (SMA), intrathecal transplantation of spinal cord-derived neural stem cells gave rise to a

small population of motoneurons and led to alleviation of neuromuscular function and motoric skills (Corti et al., 2008). Translating insights into the pathogenesis of CMT to a clinical application, particularly with the objective to use neural stem cells to replace motoneurons destroyed by the disease, is an interesting approach in this field of research. One step further towards this goal would be to investigate in a CMT mouse model whether transplantation of neuronal stem cells leads to similar success in restoring motoneurons and in improving neuromuscular function.

6 References

Abe, K., Niwa, H., Iwase, K., Takiguchi, M., Mori, M., Abé, S.I. and Yamamura, K.I. (1996), “Endoderm-specific gene expression in embryonic stem cells differentiated to embryoid bodies”, Experimental cell research, 229 pp. 27–34.

Arber, S., Han, B., Mendelsohn, M., Smith, M., Jessell, T.M. and Sockanathan, S. (1999), “Requirement for the Homeobox Gene Hb9 in the Consolidation of Motor Neuron Identity”, Neuron, 23 pp. 659–674.

Bach, D., Pich, S., Soriano, F.X., Vega, N., Baumgartner, B., Oriola, J., Daugaard, J.R., Lloberas, J., Camps, M., Zierath, J.R., Rabasa-Lhoret, R., Wallberg-Henriksson, H., Laville, M., Palacín, M., Vidal, H., Rivera, F., Brand Martin and Zorzano, A. (2003), “Mitofusin-2 Determines Mitochondrial Network Architecture and Mitochondrial Metabolism. A novel regulatory mechanism altered in obesity”, The Journal of biological chemistry, pp. 17190–17197.

Baloh, R.H., Schmidt, R.E., Pestronk, A. and Milbrandt, J. (2007), “Altered axonal mitochondrial transport in the pathogenesis of Charcot-Marie-Tooth disease from mitofusin 2 mutations”, The Journal of Neuroscience, 27 pp. 422–430.

Bartlett, J.S., Samulski, R.J. and McCown, T.J. (1998), “Selective and rapid uptake of adeno-associated virus type 2 in brain”, Human gene therapy, 9 pp. 1181–1186.

Baxter, R.V., Ben Othmane, K., Rochelle, J.M., Stajich, J.E., Hulette, C., Dew-Knight, S., Hentati, F., Ben Hamida, M., Bel, S., Stenger, J.E., Gilbert, J.R., Pericak-Vance, M.A. and Vance, J.M. (2002), “Ganglioside-induced differentiation-associated protein-1 is mutant in Charcot-Marie-Tooth disease type 4A/8q21”, Nature genetics, 30 pp. 21–22.

Bereiter-Hahn, J. (1990), “Behavior of Mitochondria in the Living Cell”, 122 pp. 1–63.

Bereiter-Hahn, J. and Vöth, M. (1994), “Dynamics of mitochondria in living cells. Shape changes, dislocations, fusion, and fission of mitochondria”, Microscopy research and technique, 27 pp. 198–219.

Branda, C.S. and Dymecki, S.M. (2004), “Talking about a Revolution”, Developmental Cell, 6 pp. 7–28.

Büning, H., Perabo, L., Coutelle, O., Quadt-Humme, S. and Hallek, M. (2008), “Recent developments in adeno-associated virus vector technology”, The journal of gene medicine, 10 pp. 717–733.

Cartoni, R., Arnaud, E., Medard, J.-J., Poirot, O., Courvoisier, D.S., Chrast, R. and Martinou, J.-C. (2010), “Expression of mitofusin 2(R94Q) in a transgenic mouse

leads to Charcot-Marie-Tooth neuropathy type 2A", Brain a journal of neurology, 133 pp. 1460–1469.

Cartoni, R. and Martinou, J.-C. (2009), "Role of mitofusin 2 mutations in the physiopathology of Charcot–Marie–Tooth disease type 2A", Experimental Neurology, 218 pp. 268–273.

Charcot, J.M. and Marie, P. (1886), "Sur une forme particulière d'atrophie musculaire progressive, souvent familiale, debutant par les pieds et les jambes et atteignant plus tard les mains", RevMéd, pp. 97–138.

Chen, H. and Chan, D.C. (2006), "Critical dependence of neurons on mitochondrial dynamics", Current Opinion in Cell Biology, 18 pp. 453–459.

Chen, H., Chomyn, A. and Chan, D.C. (2005), "Disruption of fusion results in mitochondrial heterogeneity and dysfunction", The Journal of cell biology, 280 pp. 26185–26192.

Chen, H., Detmer, S.A., Ewald, A.J., Griffin, E.E., Fraser, S.E. and Chan, D.C. (2003), "Mitofusins MFN1 and MFN2 coordinately regulate mitochondrial fusion and are essential for embryonic development", The Journal of cell biology, 160 pp. 189–200.

Chen, H., McCaffery, J.M. and Chan, D.C. (2007), "Mitochondrial fusion protects against neurodegeneration in the cerebellum", Cell, 130 pp. 548–562.

Corti, S., Nizzardo, M., Nardini, M., Donadoni, C., Salani, S., Ronchi, D., Saladino, F., Bordoni, A., Fortunato, F., Del Bo, R., Papadimitriou, D., Locatelli, F., Menozzi, G., Strazzer, S., Bresolin, N. and Comi, G.P. (2008), "Neural stem cell transplantation can ameliorate the phenotype of a mouse model of spinal muscular atrophy", The Journal of clinical investigation, 118 pp. 3316–3330.

Dalby, B., Cates, S., Harris, A., Ohki, E.C., Tilkins, M.L., Price, P.J. and Ciccarone, V.C. (2004), "Advanced transfection with Lipofectamine 2000 reagent: Primary neurons, siRNA, and high-throughput applications", Methods (San Diego, Calif.), 33 pp. 95–103.

Detmer, S.A. and Chan, D.C. (2007), "Complementation between mouse MFN1 and MFN2 protects mitochondrial fusion defects caused by CMT2A disease mutations", The Journal of cell biology, 176 pp. 405–414.

Detmer, S.A., Vande Velde, C., Cleveland, D.W. and Chan, D.C. (2008), "Hindlimb gait defects due to motor axon loss and reduced distal muscles in a transgenic mouse model of Charcot-Marie-Tooth type 2A", Human molecular genetics, 17 pp. 367–375.

Dieterlen, M.-T., Wegner, F., Schwarz, S.C., Milosevic, J., Schneider, B., Busch, M., Römuss, U., Brandt, A., Storch, A. and Schwarz, J. (2009), “Non-viral gene transfer by nucleofection allows stable gene expression in human neural progenitor cells”, Journal of neuroscience methods, 178 pp. 15–23.

Dráberová, E., Zdenek, L., Ivanyi, D., Viklický, V. and Dráber, P. (1998), “Expression of class III β-tubulin in normal and neoplastic human tissues”, Histochemistry and Cell Biology, 109 pp. 231–239.

Easter, S.S., JR., Ross, L.S. and Frankfurter, A. (1993), “Initial tract formation in the mouse brain”, The Journal of Neuroscience, ,

Evans, M.J. and Kaufman, M.H. (1981), “Establishment in culture of pluripotential cells from mouse embryos”, Nature, 292 pp. 154–156.

Fazeli, A.S., Nasrabadi, D., Pouya, A., Mirshavaladi, S., Sanati, M.H., Baharvand, H. and Salekdeh, G.H. (2013), “Proteome analysis of post-transplantation recovery mechanisms of an EAE model of multiple sclerosis treated with embryonic stem cell-derived neural precursors”, Journal of proteomics, 94 pp. 437–450.

Feely, S.M.E., Laura, M., Siskind, C.E., Sottile, S., Davis, M., Gibbons, V.S., Reilly, M.M. and Shy, M.E. (2011), “MFN2 mutations cause severe phenotypes in most patients with CMT2A”, Neurology, 76 pp. 1690–1696.

Förster, T. (1948), “Zwischenmolekulare Energiewanderung und Fluoreszenz”, Annalen der Physik, 437 pp. 55–75.

Gandre-Babbe, S. and van der Bliek, A.M. (2008), “The novel tail-anchored membrane protein Mff controls mitochondrial and peroxisomal fission in mammalian cells”, Molecular biology of the cell, 19 pp. 2402–2412.

Germond, A., Fujita, H., Ichimura, T. and Watanabe, T.M. (2016), “Design and development of genetically encoded fluorescent sensors to monitor intracellular chemical and physical parameters”, Biophysical Reviews, 8 pp. 121–138.

Gibson, D.G., Young, L., Chuang, R.-Y., Venter, J.C., Hutchison, C.A.3. and Smith, H.O. (2009), “Enzymatic assembly of DNA molecules up to several hundred kilobases”, Nature methods, 6 pp. 343–345.

Guillet, V., Gueguen, N., Cartoni, R., Chevrollier, A., Desquiret, V., Angebault, C., Amati-Bonneau, P., Procaccio, V., Bonneau, D., Martinou, J.-C. and Reynier, P. (2011), “Bioenergetic defect associated with mKATP channel opening in a mouse model carrying a mitofusin 2 mutation”, FASEB journal official publication of the Federation of American Societies for Experimental Biology, 25 pp. 1618–1627.

Hales, K.G. and Fuller, M.T. (1997), “Developmentally Regulated Mitochondrial Fusion Mediated by a Conserved, Novel, Predicted GTPase”, Cell, 90 pp. 121–129.

Harding, A.E. and Thomas, P.K. (1980), “The clinical features of hereditary motor and sensory neuropathy types I and II”, Brain a Journal of Neurology [1980, 103(2):259-280], 103 pp. 259–280.

Harel, T. and Lupski, J.R. (2014), “Charcot-Marie-Tooth disease and pathways to molecular based therapies”, Clinical Genetics, 86 pp. 422–431.

Hester, M.E., Murtha, M.J., Song, S., Rao, M., Miranda, C.J., Meyer, K., Tian, J., Boulting, G., Schaffer, D.V., Zhu, M.X., Pfaff, S.L., Gage, F.H. and Kaspar, B.K. (2011), “Rapid and efficient generation of functional motor neurons from human pluripotent stem cells using gene delivered transcription factor codes”, Molecular therapy the journal of the American Society of Gene Therapy, 19 pp. 1905–1912.

Imamura, H., Nhat, K.P.H., Togawa, H., Saito, K., Iino, R., Kato-Yamada, Y., Nagai, T. and Noji, H. (2009), “Visualization of ATP levels inside single living cells with fluorescence resonance energy transfer-based genetically encoded indicators”, Proceedings of the National Academy of Sciences, 106 pp. 15651–15656.

Itskovitz-Eldor, J., Schuldiner, M., Karsenti, D., Eden, A., Yanuka, O., Amit, M., Soreq, H. and Benvenisty, N. (2000), “Differentiation of Human Embryonic Stem Cells into Embryoid Bodies Comprising the Three Embryonic Germ Layers”, Molecular Medicine, 161 pp. 88–95.

James, D.I., Parone, P.A., Mattenberger, Y. and Martinou, J.-C. (2003), “hFis1, a novel component of the mammalian mitochondrial fission machinery”, The Journal of biological chemistry, 278 pp. 36373–36379.

Jessell, T.M. (2000), “Neuronal specification in the spinal cord- inductive signals and transcriptional codes // Neuronal specification in the spinal cord. Inductive signals and transcriptional codes”, Nature reviews. Genetics, 1 pp. 20–29.

Karra, D. and Dahm, R. (2010), “Transfection techniques for neuronal cells”, The Journal of Neuroscience, 30 pp. 6171–6177.

Keller, G.M. (1995), “In vitro differentiation of embryonic stem cells”, Current Opinion in Cell Biology, 7 pp. 862–869.

Koshiba, T., Detmer, S.A., Kaiser, J.T., Chen, H., McCaffery, J.M. and Chan, D.C. (2004), “Structural basis of mitochondrial tethering by mitofusin complexes”, Science, 305 pp. 858–862.

Kuhlenbaumer, G., Young, P., Hunermund, G., Ringelstein, B. and Stogbauer, F. (2002), “Clinical features and molecular genetics of hereditary peripheral neuropathies”, Journal of neurology, 249 pp. 1629–1650.

Kuznetsov, A.V., Hermann, M., Saks, V., Hengster, P. and Margreiter, R. (2009), “The cell-type specificity of mitochondrial dynamics”, The international journal of biochemistry & cell biology, 41 pp. 1928–1939.

Landy, A. (1989), “Dynamic, structural, and regulatory aspects of lambda site-specific recombination”, Annual review of biochemistry, 58 pp. 913–949.

Lee, Y.-j., Jeong, S.-Y., Karbowski, M., Smith, C.L. and Youle, R.J. (2004), “Roles of the mammalian mitochondrial fission and fusion mediators Fis1, Drp1, and Opa1 in apoptosis”, Molecular biology of the cell, 15 pp. 5001–5011.

Leotta, C.G., Federico, C., Brundo, M.V., Tosi, S. and Saccone, S. (2014), “HLXB9 gene expression, and nuclear location during in vitro neuronal differentiation in the SK-N-BE neuroblastoma cell line”, PloS one, 9 e105481.

Li, Z., Okamoto, K.-I., Hayashi, Y. and Sheng, M. (2004), “The importance of dendritic mitochondria in the morphogenesis and plasticity of spines and synapses”, Cell, 119 pp. 873–887.

Loiseau, D., Chevrollier, A., Verny, C., Guillet, V., Gueguen, N., Pou de Crescenzo, M.-A., Ferre, M., Malinge, M.-C., Guichet, A., Nicolas, G., Amati-Bonneau, P., Malthiery, Y., Bonneau, D. and Reynier, P. (2007), “Mitochondrial coupling defect in Charcot-Marie-Tooth type 2A disease”, Annals of neurology, 61 pp. 315–323.

Lu, P., Woodruff, G., Wang, Y., Graham, L., Hunt, M., Di Wu, Boehle, E., Ahmad, R., Poplawski, G., Brock, J., Goldstein, L.S.B. and Tuszynski, M.H. (2014), “Long-distance axonal growth from human induced pluripotent stem cells after spinal cord injury”, Neuron, 83 pp. 789–796.

Martin, G.R. (1981), “Isolation of a pluripotent cell line from early mouse embryos cultured in medium conditioned by teratocarcinoma stem cells”, Proceedings of the National Academy of Sciences, 78 pp. 7634–7638.

Mattie, S., Riemer, J., Wideman, J.G. and McBride, H.M. (2018), “A new mitofusin topology places the redox-regulated C terminus in the mitochondrial intermembrane space”, The Journal of cell biology, 217 pp. 507–515.

Mazzoni, E.O., Mahony, S., Closser, M., Morrison, C.A., Nedelec, S., Williams, D.J., An, D., Gifford, D.K. and Wichterle, H. (2013), “Synergistic binding of transcription factors to cell-specific enhancers programs motor neuron identity”, Nature Neuroscience, 16 pp. 1219–1227.

Mears, J.A., Lackner, L.L., Fang, S., Ingerman, E., Nunnari, J. and Hinshaw, J.E. (2011), “Conformational changes in Dnm1 support a contractile mechanism for mitochondrial fission”, Nature structural & molecular biology, 18 pp. 20–26.

Meeusen, S., DeVay, R., Block, J., Cassidy-Stone, A., Wayson, S., McCaffery, J.M. and Nunnari, J. (2006), “Mitochondrial inner-membrane fusion and crista maintenance requires the dynamin-related GTPase Mgm1”, Cell, 127 pp. 383–395.

Misko, A., Jiang, S., Wegorzewska, I., Milbrandt, J. and Baloh, R.H. (2010), “Mitofusin 2 is necessary for transport of axonal mitochondria and interacts with the Miro/Milton complex”, The Journal of neuroscience the official journal of the Society for Neuroscience, 30 pp. 4232–4240.

Mitalipova, M., Calhoun, J., Shin, S., Wininger, D., Schulz, T., Noggle, S., Venable, A., Lyons, I., Robins, A. and Stice, S. (2003), “Human embryonic stem cell lines derived from discarded embryos”, Stem cells (Dayton, Ohio), 21 pp. 521–526.

Murgia, M., Giorgi, C., Pinton, P. and Rizzuto, R. (2009), “Controlling metabolism and cell death. At the heart of mitochondrial calcium signalling”, Journal of molecular and cellular cardiology, 46 pp. 781–788.

Nakada, K., Inoue, K., Ono, T., Isobe, K., Ogura, A., Goto, Y.I., Nonaka, I. and Hayashi, J.I. (2001), “Inter-mitochondrial complementation. Mitochondria-specific system preventing mice from expression of disease phenotypes by mutant mtDNA”, Nature medicine, 7 pp. 934–940.

Okabe, S., Forsberg-Nilsson, K., Spiro, A.C., Segal, M. and McKay, R.D. (1996), “Development of neuronal precursor cells and functional postmitotic neurons from embryonic stem cells in vitro”, Mechanisms of Development, 59 pp. 89–102.

Palade, G.E. (1953), “AN ELECTRON MICROSCOPE STUDY OF THE MITOCHONDRIAL STRUCTURE”, Journal of Histochemistry & Cytochemistry, ,

Pepperkok, R. and Ellenberg, J. (2006), “High-throughput fluorescence microscopy for systems biology”, Nature reviews. Molecular cell biology, 7 pp. 690–696.

Pfaff, S.L., Mendelsohn, M., Stewart, C.L., Edlund, T. and Jessell, T.M. (1996), “Requirement for LIM Homeobox Gene Isl1 in Motor Neuron Generation Reveals a Motor Neuron– Dependent Step in Interneuron Differentiation”, Cell, 84 pp. 309–320.

Pich, S., Bach, D., Briones, P., Liesa, M., Camps, M., Testar, X., Palacin, M. and Zorzano, A. (2005), “The Charcot-Marie-Tooth type 2A gene product, MFN2, up-

regulates fuel oxidation through expression of OXPHOS system", Human molecular genetics, 14 pp. 1405–1415.

Rippon, H.J. and Bishop, A.E. (2004), "Embryonic stem cells", Cell Proliferation, 37 pp. 23–34.

Rojo, M., Legros, F., Chateau, D. and Lombès, A. (2002), "Membrane topology and mitochondrial targeting of mitofusins, ubiquitous mammalian homologs of the transmembrane GTPase Fzo", Journal of Cell Science, pp. 1663–1674.

Royo, N.C., Vandenberghe, L.H., Ma, J.-Y., Hauspurg, A., Yu, L., Maronski, M., Johnston, J., Dichter, M.A., Wilson, J.M. and Watson, D.J. (2008), "Specific AAV serotypes stably transduce primary hippocampal and cortical cultures with high efficiency and low toxicity", Brain research, 1190 pp. 15–22.

San Martin, A., Ceballo, S., Ruminot, I., Lerchundi, R., Frommer, W.B. and Barros, L.F. (2013), "A genetically encoded FRET lactate sensor and its use to detect the Warburg effect in single cancer cells", PloS one, 8 e57712.

Santel, A. (2006), "Get the balance right. Mitofusins roles in health and disease", Biochimica et biophysica acta, 1763 pp. 490–499.

Santel, A., Frank, S., Gaume, B., Herrler, M., Youle, R.J. and Fuller, M.T. (2003), "Mitofusin-1 protein is a generally expressed mediator of mitochondrial fusion in mammalian cells", Journal of Cell Science, 116 pp. 2763–2774.

Santel, A. and Fuller, M.T. (2001), "Control of mitochondrial morphology by a human mitofusin", Journal of Cell Science, pp. 867–874.

Sato, A., Nakada, K. and Hayashi, J.-I. (2006), "Mitochondrial dynamics and aging. Mitochondrial interaction preventing individuals from expression of respiratory deficiency caused by mutant mtDNA", Biochimica et biophysica acta, 1763 pp. 473–481.

Schon, E.A. and Przedborski, S. (2011), "Mitochondria. The Next (Neurode)Generation", Neuron, 70 pp. 1033–1053.

Sesaki, H. and Jensen, R.E. (1999), "Division versus Fusion. Dnm1p and Fzo1p Antagonistically Regulate Mitochondrial Shape", The Journal of cell biology, 147 pp. 699–706.

Skre, H. (1974), "Genetic and clinical aspects of Charcot-Marie-Tooth's disease", Clinical Genetics, 6 pp. 98–118.

Skulachev, V.P. (2001), "Mitochondrial filaments and clusters as intracellular power-transmitting cables", Trends in Biochemical Sciences, 26 pp. 23–29.

Smirnova, E., Griparic, L., Shurland, D.-L. and van der Bliek, A.M. (2001), “Dynamin-related Protein Drp1 Is Required for Mitochondrial Division in Mammalian Cells”, Molecular biology of the cell, 12 pp. 2245–2256.

Smith, A.G. (2001), “Embryo-Derived Stem Cells: Of Mice and Men”, Annual Review of Cell and Developmental, pp. 435–462.

Sohal, V.S., Zhang, F., Yizhar, O. and Deisseroth, K. (2009), “Parvalbumin neurons and gamma rhythms enhance cortical circuit performance”, Nature, 459 pp. 698–702.

Song, Z., Ghochani, M., McCaffery, J.M., Frey, T.G. and Chan, D.C. (2009), “Mitofusins and OPA1 mediate sequential steps in mitochondrial membrane fusion”, Molecular biology of the cell, 20 pp. 3525–3532.

Takahashi, K., Tanabe, K., Ohnuki, M., Narita, M., Ichisaka, T., Tomoda, K. and Yamanaka, S. (2007), “Induction of pluripotent stem cells from adult human fibroblasts by defined factors”, Cell, 131 pp. 861–872.

Thomson, J.A. (1998), “Embryonic Stem Cell Lines Derived from Human Blastocysts”, Science, 282 pp. 1145–1147.

Tondera, D., Grandemange, S., Jourdain, A., Karbowski, M., Mattenberger, Y., Herzig, S., Da Cruz, S., Clerc, P., Raschke, I., Merkwirth, C., Ehses, S., Krause, F., Chan, D.C., Alexander, C., Bauer, C., Youle, R., Langer, T. and Martinou, J.-C. (2009), “SLP-2 is required for stress-induced mitochondrial hyperfusion”, The EMBO journal, 28 pp. 1589–1600.

Tooth, H.H. (1886), “The perone type of progressive muscular atrophy”, London: HK Lewis and Co, ,

van Hameren, G., Campbell, G., Deck, M., Berthelot, J., Gautier, B., Quintana, P., Chrast, R. and Tricaud, N. (2019), “In vivo real-time dynamics of ATP and ROS production in axonal mitochondria show decoupling in mouse models of peripheral neuropathies”, Acta neuropathologica communications, 7 p. 86.

Verhoeven, K., Claeys, K.G., Züchner, S., Schröder, J.M., Weis, J., Ceuterick, C., Jordanova, A., Nelis, E., Vriendt, E. de, van Hul, M., Seeman, P., Mazanec, R., Saifi, G.M., Szigeti, K., Mancias, P., Butler, I.J., Kochanski, A., Ryniewicz, B., Bleecker, J. de, van den Bergh, P., Verellen, C., van Coster, R., Goemans, N., Auer-Grumbach, M., Robberecht, W., Milic Rasic, V., Nevo, Y., Tournev, I., Guergueltcheva, V., Roelens, F., Vieregge, P., Vinci, P., Moreno, M.T., Christen, H.-J., Shy, M.E., Lupski, J.R., Vance, J.M., Jonghe, P.D. and Timmerman, V.

(2006), “MFN2 mutation distribution and genotype/phenotype correlation in Charcot-Marie-Tooth type 2”, Brain a journal of neurology, 129 pp. 2093–2102.

Verstreken, P., Ly, C.V., Venken, K.J.T., Koh, T.-W., Zhou, Y. and Bellen, H.J. (2005), “Synaptic mitochondria are critical for mobilization of reserve pool vesicles at Drosophila neuromuscular junctions”, Neuron, 47 pp. 365–378.

Wagers, A.J., Christensen, J.L. and Weissman, I.L. (2002), “Cell fate determination from stem cells”, Gene therapy, 9 pp. 606–612.

Washbourne, P. and McAllister, A. (2002), “Techniques for gene transfer into neurons”, Current Opinion in Neurobiology, 12 pp. 566–573.

Westermann, B. (2012), “Bioenergetic role of mitochondrial fusion and fission”, Biochimica et biophysica acta, 1817 pp. 1833–1838.

Wichterle, H., Lieberam, I., Porter, J.A. and Jessell, T.M. (2002), “Directed Differentiation of Embryonic Stem Cells into Motor Neurons”, Cell, 110 pp. 385–397.

Williams, R.L., Hilton, D.J., Pease, S., Willson, T.A., Stewart, C.L., Gearing, D.P., Wagner, E.F., Metcalf, D., Nicola, N.A. and Gough, N.M. (1988), “Myeloid leukaemia inhibitory factor maintains the developmental potential of embryonic stem cells”, Nature, 336 pp. 684–687.

Wolf, C., Zimmermann, R., Thaher, O., Bueno, D., Wüllner, V., Schäfer, M.K.E., Albrecht, P. and Methner, A. (2019), “The Charcot-Marie Tooth Disease Mutation R94Q in MFN2 Decreases ATP Production but Increases Mitochondrial Respiration under Conditions of Mild Oxidative Stress”, Cells, 8

Zuchner, S., Mersiyanova, I.V., Muglia, M., Bissar-Tadmouri, N., Rochelle, J., Dadali, E.L., Zappia, M., Nelis, E., Patitucci, A., Senderek, J., Parman, Y., Evgrafov, O., Jonghe, P.D., Takahashi, Y., Tsuji, S., Pericak-Vance, M.A., Quattrone, A., Battaloglu, E., Polyakov, A.V., Timmerman, V., Schroder, J.M. and Vance, J.M. (2004), “Mutations in the mitochondrial GTPase mitofusin 2 cause Charcot-Marie-Tooth neuropathy type 2A”, Nature genetics, 36 pp. 449–451.

7 Attachment

7.1 Acknowledgement

7.2 Curriculum Vitae